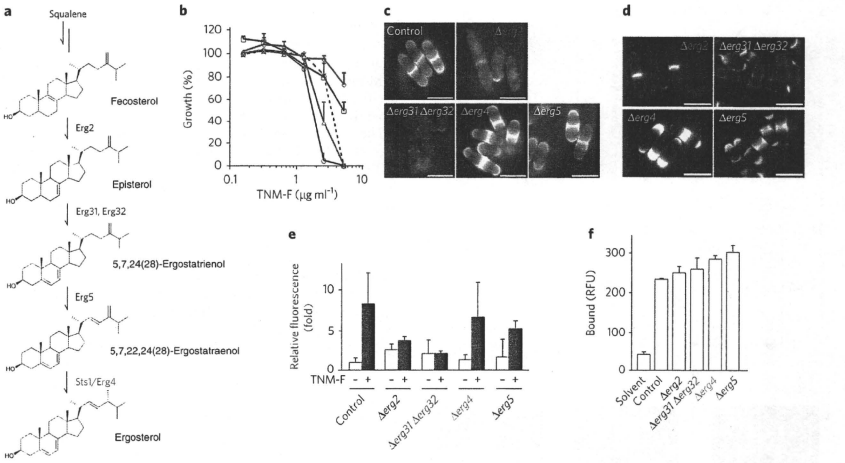

Figure 4 | Genetic interactions with ergosterol biosynthetic genes. (**a**) Ergosterol biosynthesis pathway. (**b**) TNM-F sensitivity of *erg* mutants, *Δerg2* (solid blue); *Δerg31 Δerg32* (solid red); *Δsts1/erg4* (solid green); *Δerg5* (dashed black); and the control strain HM123 (solid black). Data represent means of three independent experiments. Error bars, s.d. (**c**) Localization of TNM-BF-binding molecules in *erg* mutant cells. Cells were treated with TNM-BF (2.5 μg ml^{-1}) at 30 °C for 1 h, and the fluorescence was observed. (**d**,**e**) Effects of mutations in the ergosterol biosynthetic pathway on the TNM-F-induced cell wall abnormality. Various *erg* mutants were treated with TNM-F, and the extent of abnormal cell wall synthesis was determined using Cfw staining. Quantitation of the fluorescence intensity is shown in **e**. Relative intensities to the control cells treated with DMSO were determined. Error bars represent s.d. of three independent experiments ($n \geq 9$ for each experiment). (**f**) Binding of TNM-BF to the sterol fractions prepared from various *erg* mutant cells. Data represent means of three independent experiments. Error bars, s.d.; scale bars, 10 μm.

reaction from episterol to 5,7,24(28)-ergostatrienol, caused ergosterol deficiency and apparent tolerance to polyene antibiotics[27]. These *erg* mutants were also highly tolerant to TNM-F (**Fig. 4b**). On the other hand, deletion of *erg5* conferred modest resistance to TNM-F, and only marginal resistance was observed in *Δsts1/erg4* cells (**Fig. 4b**). However, deletion of *dsd1* (ref. 36) or *SPBC887.15c*, both encoding enzymes involved in sphingolipid metabolism, did not affect the sensitivity to TNM-F. But *ΔSPBC887.15c* cells were specifically resistant to syringomycin E (**Supplementary Fig. 15**). The ability of TNM-BF to bind to cells correlated well with their sensitivity to TNM-F (**Fig. 4c**). The extent of the abnormality in cell wall architecture in the TNM-F-treated *erg* mutant cells correlated with their TNM sensitivity as well as binding capacity (**Fig. 4d**,**e** and **Supplementary Fig. 16**). However, *in vitro* binding experiments showed similar TNM-BF binding of the sterol fractions isolated from all *erg* deletion strains (**Fig. 4f**), indicating that TNMs bind to other cellular sterols *in vitro*. It is likely that changes in the state of the plasma membrane in the *erg* mutants render TNM-F less readily accessible to membrane sterols. Indeed, the ability to bind to filipin was also reduced in the *Δerg2* and *Δerg31 Δerg32* cells (**Supplementary Fig. 17**)[27], indicating the modulated accessibility of 3β-hydroxysterols in the membrane of these mutants.

Effects of TNM-F on plasma membrane integrity

To further examine whether TNM binding of the sterol-rich membrane affects yeast plasma membrane integrity, we added the fluorescent dye calcein to the *S. pombe* cells that had been treated with TNM-F for 9 h. Passive entry of calcein over the plasma membrane was observed upon treatment with TNM-F, indicating that cells cannot retain the membrane integrity in the presence of TNM-F (**Fig. 5a**). Calcein diffusion following TNM-F exposure increased in a dose-dependent manner (**Fig. 5b**). Time-course experiments showed that the calcein diffusion into the TNM-F–treated cells gradually increased over time (**Fig. 5c**). In contrast, the elevated 1,3-β-D-glucan synthesis occurred very rapidly, and 1 h treatment was sufficient for the induction of 1,3-β-D-glucan synthesis in most cells at the concentration of 5 μg ml^{-1} (**Supplementary Fig. 18**). Consistent with the TNM susceptibility (**Fig. 4b**), binding (**Fig. 4c**) and Cfw staining (**Fig. 4d**,**e**) data, no significant diffusion of calcein was observed in *Δerg2* and *Δerg31 Δerg32* cells (**Fig. 5d**), suggesting a direct link between TNM-F binding and the observed effects, including loss of membrane integrity.

Comparison with polyene antifungals

Lastly, we asked whether the mode of action of TNM is identical to that of the conventionally used polyene antibiotics. The most typical morphological change of yeast cells after treatment with polyene antibiotics is the enlargement of vacuoles (**Fig. 5e**,**f**)[37]. This phenomenon was not observed in the TNM-F–treated cells; instead, the vacuoles became highly fragmented (**Fig. 5g**). In contrast to the vacuoles of AMB-treated cells, which leaked vacuolar-specific dye (CDCFDA) to the cytosol, the fragmented vacuoles in the TNM-F-treated cells retained the dye, suggesting that the vacuolar membrane damage is marginal. Rho1 may also be involved in vacuole fragmentation induced by TNM because overexpression of wild-type Rho1 caused similar vacuole fragmentation, and Rho1T20N alleviated the TNM-induced vacuole abnormality (**Supplementary Fig. 19**).

The other characteristic aspect of polyene antifungals is their acute fungicidal effect: most cells died shortly after AMB treatment, and no

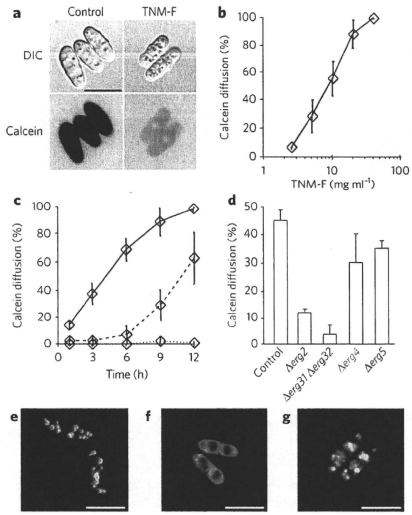

Figure 5 | Disruption of plasma membrane integrity by TNM-F. (**a**) Dye exclusion assay for testing plasma membrane integrity using calcein, a membrane-impermeable fluorescent dye. Passive entry of calcein into *S. pombe* cells was induced by TNM-F (20 μg ml^{-1} for 9 h). In the absence of TNM-F, calcein diffusion was rarely observed. (**b**,**c**) Kinetics of calcein diffusion induced by TNM-F. The dye diffusion was observed in a manner dependent on concentration (**b**) and time (**c**). Incubation time in **b** was 9 h. Cells were incubated without (dotted line) or with 5 μg ml^{-1} (dashed line) or 20 μg ml^{-1} (solid line) of TNM-F in **c**. (**d**) Effects of *erg* mutations on TNM-F–induced membrane damage. Calcein diffusion was attenuated in *Δerg2* or *Δerg31 Δerg32* cells. Data in **b**-**d** represent means of three independent experiments ($n > 10$ for each experiment). Error bars, s.d. (**e**-**g**) Changes in vacuole morphology. Wild-type cells stained with CDCFDA (green) and FM4-64 (red) were exposed to DMSO (**e**, 1% (v/v)), AMB (**f**, 5 μg ml^{-1}) or TNM-F (**g**, 10 μg ml^{-1}) for 1 h. Scale bars, 10 μm.

time-dependent cell death was observed (**Supplementary Fig. 20**). In contrast, TNM-F showed time-dependent toxicity, with similar kinetics to that of the calcein diffusion (**Fig. 5c** and **Supplementary Fig. 20**). Taken together with the inability of AMB or nystatin to increase 1,3-β-D-glucan synthesis (**Fig. 2g**), these data caused us to conclude that TNM-F is a previously undescribed sterol-binding molecule and that its mode of action is distinct from that of polyene antibiotics.

DISCUSSION

Marine invertebrates, including marine sponges, are an important source for numerous biologically active compounds, which are often synthesized by symbiotic microorganisms[38]. Bicyclic peptides, such as theonellamides (TNMs), are a family of marine natural products with potent antifungal activity. Despite extensive efforts to isolate the TNM-binding proteins, the modes of action of these compounds have been heretofore unknown. Recently, a mutation in *MVD1*, also known as *ERG19*, encoding an essential enzyme involved in an early step in the ergosterol biosynthesis pathway was shown to be specifically resistant to theopalauamide in *Saccharomyces cerevisiae*[39], suggesting a link between the drug target and the ergosterol biosynthetic pathway. In this study, by taking advantage of a chemical-genomic screen for the genes that alter TNM sensitivity when overexpressed, we demonstrated that TNM specifically binds to a class of lipid molecules (3β-hydroxysterols), rather than a protein, in the fission yeast.

The idea that ergosterol, the major sterol molecule in fungi, is the target of TNM in fission yeast is supported not only by the compound's physical interaction with 3β-hydroxysterols, including ergosterol, but also by several lines of genetic and biochemical evidence. Mutants defective in ergosterol biosynthesis (*Δerg2* and *Δerg31 Δerg32*) showed drastically increased tolerance to TNM and a decreased ability of the cells to bind TNM. Drug sensitivity was well correlated with *in vivo* TNM binding of the membrane. Indeed, TNM-BF binding of the cells overexpressing *SPCC23B6.04c*, the gene conferring the highest resistance, was very low (**Supplementary Fig. 12**). In contrast, *in vitro* binding of TNM-BF to the extracted sterol fraction was independent of susceptibilities of the *erg* mutants, suggesting that TNM-BF binds to sterol metabolites other than ergosterol *in vitro*, and that the accessibility of these 3β-hydroxysterols and the membrane architectures determine the efficient binding of TNM to the plasma membrane *in vivo*. The observation that defects in actin impaired polarized distribution of sterols[30] and greatly reduced *in vivo* TNM binding also supports the notion that proper organization of the membrane domain is prerequisite for *in vivo* TNM binding of the membrane sterols.

TNM binding 3β-hydroxysterols in the membrane initially induced overproduction of the cell wall component 1,3-β-D-glucan. *S. pombe* Rho1 GTPase regulates 1,3-β-D-glucan synthase and is required for the maintenance of cell wall integrity and polarization of the actin cytoskeleton[21,23]. Our mutational analyses demonstrated that TNM triggers the onset of signaling mediated by Rho1 GTPase to directly activate 1,3-β-D-glucan synthase. TNM treatment led to rapid accumulation of 1,3-β-D-glucan at the cell tips and the site of cytokinesis (**Fig. 5c** and **Supplementary Fig. 18**), which are essentially the same regions stained by filipin and TNM-BF, implying that 1,3-β-D-glucan synthase is also localized within or adjacent to the lipid microdomains. Rho1 may also be involved in vacuole fragmentation induced by TNM (**Supplementary Fig. 19**).

A later biological consequence of TNM binding the sterol-rich membrane was the induction of membrane damage. Indeed, the dye exclusion assay showed that the integrity of the plasma membrane in *S. pombe* was damaged by TNM in an incubation time–dependent manner, thereby reducing cell viability. Although TNM induced aberrant 1,3-β-D-glucan synthesis by Rho1 activation, it may be independent of the TNM-induced cytotoxic membrane damage, as the overexpression of Rho1T20N did not suppress the TNM-BF binding the cell membrane (**Supplementary Fig. 7**) and cytotoxicity of TNM-F (**Supplementary Fig. 8**). The polyene antifungals also form pores in the lipid bilayer by interacting with ergosterol, thereby causing leakage of cytosolic constituents such as ions[40]. However, the mode of action of TNM-F is apparently distinct from that of polyene antifungals because the phenotypic changes induced by these two families of antifungals are different. Not all the *erg* mutants prevented TNM binding and damage to membrane. What has been established is the correlation between the TNM's effects on cells and its efficient binding to plasma membrane *in vivo* (**Fig. 4** and **Supplementary Fig. 12**). It is most likely that the binding of TNM-F requires not only sufficient content of ergosterol and other 3β-hydroxysterols but also the proper membrane architecture. In that sense, TNM resembles lysenin, a sphingomyelin-specific toxin isolated from the coelomic fluid of the earthworm *Eisenia foetida*, which has been shown to bind clusters of sphingomyelin in the membrane[41]. Thus, TNM represents a previously unknown class of sterol-binding molecules.

In summary, we have discovered that TNM represents a previously undescribed, mechanistically distinct class of sterol-binding molecules, a powerful tool for exploring the function and localization of sterols in cells. It remains to be determined how TNM binds to sterols in plasma membrane *in situ* and activates Rho1-mediated 1,3-β-D-glucan synthesis, as well as other processes that lead subsequently to membrane damage and cytotoxicity. To develop practical antifungal drugs from such large and complex natural products, it will also be critical to perform structure-function relationship studies to identify the minimal chemical structure essential for TNM's biological activity.

METHODS

Chemical compounds. Thiabendazole and damnacanthal were purchased from Wako Pure Chemical Industries. Other compounds for chemical-genomic profiling were purchased from Sigma. FK463 and cispentacin were gifts from A. Fujie, Astellas Pharma. Trichostatin A and FK228 were from the laboratory collection. TNM-F was isolated from a marine sponge *Theonella* sp. as described previously[8]. The fluorescent derivative of TNM was prepared as described in the **Supplementary Methods.** 1,2-Dimyristoyl-*sn*-glycero-3-phosphocholine (DMPC), 1,2-dimyristoyl-*sn*-glycero-3-phosphoethanolamine (DMPE), and methyl-β-cyclodextrin were purchased from Wako Pure Chemical Industries, Ltd. 1-Palmitoyl-2-oleoyl-*sn*-glycero-3-phosphocholine (POPC), 1,2-dimyristoyl-*sn*-glycero-3-phospho-L-serine (DMPS), chicken egg yolk sphingomyelin (SM), cholesterol, cholestanol, 5α-cholest-7-en-3β-ol, cholesteryl acetate, 5α-cholestan-3-on, 5α-cholestane, calcofluor white, filipin, latrunculin A and syringomycin E were from Sigma. Ergosterol was from Nacalai Tesque, 5-cholesten-3α-ol was from Steraloids Inc., calcein was from Dojindo Laboratories and CDCFDA and FM4-64 were from Molecular Probes Inc.

Yeast strains. *S. pombe* strains used in this study are JY1 (h^-), HM123 (h^- *leu1-32*), *erg* mutants (h^- *ura4-C190T leu1-32 erg2::ura4*$^+$, h^- *ura4-C190T leu1-32 erg3l::ura4*-FOA[b] *erg32::ura4*$^+$, h^- *ura4-C190T leu1-32 erg4::ura4*$^+$, and h^- *ura4-C190T leu1-32 erg5::ura4*$^+$)[27], and KP165 (h^- *leu1-32 bgs1-i2*)[19]. Fission yeast overexpression strains derived from AM2 (h^{90} *leu1-32*) were generated using the multipurpose plasmid pDUAL-FFH1c[42] as described previously[13].

Preparation of chemical-genomic profiles. Overexpression strains were initially grown on SD solid medium at 30 °C for 2–3 d. To allow expression, each strain was subsequently grown in 200 μL of minimal medium in 96-well plates at 30 °C for 48 h with vigorous shaking. Expression-induced cell cultures were diluted at 1:2,000 and exposed to compounds at 30 °C for 24 h in 100 μL minimal medium in 96-well plates. Cell growth was assessed by the degree of respiration (an XTT assay) using a Cell Proliferation Kit II (Roche, Switzerland). Secondary screens were carried out on strains showing significantly altered sensitivity in the primary screen. The sensitivity of the strain was quantified by calculating the area under the curve (AUC) of growth versus dose (*x* axis: compound concentration; *y* axis: cell growth (%)), normalized against the median AUC value of all strains in each experiment. Strains with significantly altered normalized AUC values in the secondary screen were tested again; in this trial, the obtained AUC value was normalized against the AUC value from the control strain (**Supplementary Data Sets 2** and **3**).

Preparation of compound profiles using a minimal strain set. See **Supplementary Methods** for experimental procedures.

Clustering analysis. See **Supplementary Methods** and **Supplementary Dataset 8** for experimental procedures.

Functional analysis of the chemical-genomic profiles with GO terms. See **Supplementary Methods** for experimental procedures.

Lipid binding assay. The ability of TNM-BF to bind to various lipid species was evaluated in a microtiter plate. The wells of microtiter plates (Immulon 1B, Thermo Fisher Scientific, Inc.) were coated with lipid solution (50 μM of DMPC, DMPE, DMPS, sterols (10 μM each), SM (10 μg ml^{-1}), or 40 μl of yeast sterol fractions (10 μg ml^{-1})) in ethanol by evaporating at 30 °C for 2 h. After blocking the wells with Tris-buffered saline (10 mM Tris-HCl, pH 7.4, 150 mM NaCl) containing 1% (v/v) skim milk (BD) (buffer A) for 1 h at 30 °C, the wells were incubated with TNM-BF (1.0 μg ml^{-1}) in buffer A for 1 h at 30 °C. After washing the wells twice with buffer A, we dissolved the bound TNM-BF in 50 μl of DMSO, 40 μl of which was transferred to another 96-well plate (FIA black module plate, Greiner Bio-One) to measure the bound fluorescence (excitation 490 nm, emission 528 nm) using a SpectraMax M2e microplate reader (Molecular Devices). Yeast sterol fractions were prepared as described previously[27].

Drug sensitivity test. See **Supplementary Methods** for experimental procedures.

Microscopy. Cells were treated with compounds at 30 °C unless stated otherwise in the figure legend. Multilamellar vesicle competition was carried out using POPC-based vesicles. In detail, TNM-F (10 μg ml^{-1}) was preincubated with POPC vesicles or POPC-based vesicles (100 μM of total lipid concentration) containing 20 mol % of DMPE, DMPS, SM or ergosterol for 30 min. Cells were incubated with this mixture for 3 h (final concentration of TNM-F is 5 μg ml^{-1} and that of total lipid is 50 μM), then fixed and stained with Cfw. For Cfw staining, fixed cells were suspended in a buffer (100 mM PIPES, pH 6.9, 1 mM EGTA, 1 mM $MgSO_4$) containing Cfw. Cell lysis by FK463 was observed as described in **Supplementary Methods.** Visualization of sterols using filipin was carried out as described[29]. For the co-localization study, cells were exposed to TNM-BF (2.5 μg ml^{-1}) for 30 min, followed by filipin staining. Vacuole morphology was visualized with FM4-64 and CDCFDA as described[43]. Dye exclusion assay was carried in the presence of calcein at a concentration of 50 μg ml^{-1}. To collect images, we used either a DeltaVision system (Applied Precision) with an Olympus IX70 fluorescence microscope equipped with an UPlan Apo ×100 lens, or a MetaMorph system (Universal Imaging Corp.) with an Olympus IX81 fluorescence microscope equipped with an UPLSAPO ×100 lens. Quantitation of the intensity of the Cfw fluorescence was carried out using MetaMorph software.

Received 6 February 2009; accepted 23 March 2010; published online 13 June 2010

References

1. Baltz, R.H. Daptomycin: mechanisms of action and resistance, and biosynthetic engineering. *Curr. Opin. Chem. Biol.* **13**, 144–151 (2009).
2. Denning, D.W. Echinocandin antifungal drugs. *Lancet* **362**, 1142–1151 (2003).
3. Rovira, P., Mascarell, L. & Truffa-Bachi, P. The impact of immunosuppressive drugs on the analysis of T-cell activation. *Curr. Med. Chem.* **7**, 673–692 (2000).
4. Dawson, S., Malkinson, J.P., Paumier, D. & Searcey, M. Bisintercalator natural products with potential therapeutic applications: isolation, structure determination, synthetic and biological studies. *Nat. Prod. Rep.* **24**, 109–126 (2007).
5. Kong, D. *et al.* Echinomycin, a small-molecule inhibitor of hypoxia-inducible factor-1 DNA-binding activity. *Cancer Res.* **65**, 9047–9055 (2005).
6. Vera, M.D. & Joullie, M.M. Natural products as probes of cell biology: 20 years of didemnin research. *Med. Res. Rev.* **22**, 102–145 (2002).
7. Matsunaga, S. & Fusetani, N. Nonribosomal peptides from marine sponges. *Curr. Org. Chem.* **7**, 945–966 (2003).
8. Matsunaga, S., Fusetani, N., Hashimoto, K. & Walchli, M. Theonellamide-F - a novel antifungal bicyclic peptide from a marine sponge *Theonella* sp. *J. Am. Chem. Soc.* **111**, 2582–2588 (1989).
9. Matsunaga, S. & Fusetani, N. Theonellamides A–E, cytotoxic bicyclic peptides, from a marine sponge *Theonella* sp. *J. Org. Chem.* **60**, 1177–1181 (1995).
10. Bewley, C.A. & Faulkner, D.J. Theonegramide, an antifungal glycopeptide from the Philippine lithistid sponge *Theonella swinhoei*. *J. Org. Chem.* **59**, 4849–4852 (1994).
11. Schmidt, E.W., Bewley, C.A. & Faulkner, D.J. Theopalauamide, a bicyclic glycopeptide from filamentous bacterial symbionts of the lithistid sponge *Theonella swinhoei* from Palau and Mozambique. *J. Org. Chem.* **63**, 1254–1258 (1998).
12. Wada, S., Matsunaga, S., Fusetani, N. & Watabe, S. Interaction of cytotoxic bicyclic peptides, theonellamides A and F, with glutamate dehydrogenase and 17beta-hydroxysteroid dehydrogenase IV. *Mar. Biotechnol. (NY)* **2**, 285–292 (2000).
13. Matsuyama, A. *et al.* ORFeome cloning and global analysis of protein localization in the fission yeast *Schizosaccharomyces pombe*. *Nat. Biotechnol.* **24**, 841–847 (2006).
14. Shirai, A. *et al.* Global analysis of gel mobility of proteins and its use in target identification. *J. Biol. Chem.* **283**, 10745–10752 (2008).
15. Kanoh, N., Honda, K., Simizu, S., Muroi, M. & Osada, H. Photo-cross-linked small-molecule affinity matrix for facilitating forward and reverse chemical genetics. *Angew. Chem. Int. Edn Engl.* **44**, 3559–3562 (2005).
16. Hughes, T.R. *et al.* Functional discovery via a compendium of expression profiles. *Cell* **102**, 109–126 (2000).
17. Arellano, M. *et al. Schizosaccharomyces pombe* protein kinase C homologues, pck1p and pck2p, are targets of rho1p and rho2p and differentially regulate cell integrity. *J. Cell Sci.* **112**, 3569–3578 (1999).
18. Tomishima, M. *et al.* FK463, a novel water-soluble echinocandin lipopeptide: synthesis and antifungal activity. *J. Antibiot. (Tokyo)* **52**, 674–676 (1999).
19. Deng, L. *et al.* Phosphatidylinositol-4-phosphate 5-kinase regulates fission yeast cell integrity through a phospholipase C-mediated protein kinase C-independent pathway. *J. Biol. Chem.* **280**, 27561–27568 (2005).
20. Kippert, F. & Lloyd, D. The aniline blue fluorochrome specifically stains the septum of both live and fixed *Schizosaccharomyces pombe* cells. *FEMS Microbiol. Lett.* **132**, 215–219 (1995).
21. Arellano, M., Duran, A. & Perez, P. Rho 1 GTPase activates the (1–3) beta-D-glucan synthase and is involved in *Schizosaccharomyces pombe* morphogenesis. *EMBO J.* **15**, 4584–4591 (1996).

22. Arellano, M., Duran, A. & Perez, P. Localisation of the *Schizosaccharomyces pombe* rho1p GTPase and its involvement in the organisation of the actin cytoskeleton. *J. Cell Sci.* **110**, 2547–2555 (1997).
23. Nakano, K., Arai, R. & Mabuchi, I. The small GTP-binding protein Rho1 is a multifunctional protein that regulates actin localization, cell polarity, and septum formation in the fission yeast *Schizosaccharomyces pombe*. *Genes Cells* **2**, 679–694 (1997).
24. Sayers, L.G. *et al.* Rho-dependence of *Schizosaccharomyces pombe* Pck2. *Genes Cells* **5**, 17–27 (2000).
25. Takeda, T., Kawate, T. & Chang, F. Organization of a sterol-rich membrane domain by cdc15p during cytokinesis in fission yeast. *Nat. Cell Biol.* **6**, 1142–1144 (2004).
26. Simons, K. & Ikonen, E. Functional rafts in cell membranes. *Nature* **387**, 569–572 (1997).
27. Iwaki, T. *et al.* Multiple functions of ergosterol in the fission yeast *Schizosaccharomyces pombe*. *Microbiology* **154**, 830–841 (2008).
28. Drabikowski, W., Lagwińska, E. & Sarzala, M.G. Filipin as a fluorescent probe for location of cholesterol in membranes of fragmented sarcoplasmic reticulum. *Biochim. Biophys. Acta* **291**, 61–70 (1973).
29. Wachtler, V., Rajagopalan, S. & Balasubramanian, M.K. Sterol-rich plasma membrane domains in the fission yeast *Schizosaccharomyces pombe*. *J. Cell Sci.* **116**, 867–874 (2003).
30. Codlin, S., Haines, R.L. & Mole, S.E. btn1 affects endocytosis, polarization of sterol-rich membrane domains and polarized growth in *Schizosaccharomyces pombe*. *Traffic* **9**, 936–950 (2008).
31. Ishiguro, J. & Kobayashi, W. An actin point-mutation neighboring the 'hydrophobic plug' causes defects in the maintenance of cell polarity and septum organization in the fission yeast *Schizosaccharomyces pombe*. *FEBS Lett.* **392**, 237–241 (1996).
32. Villar-Tajadura, M.A. *et al.* Rga2 is a Rho2 GAP that regulates morphogenesis and cell integrity in *S. pombe*. *Mol. Microbiol.* **70**, 867–881 (2008).
33. Chang, E.C. *et al.* Cooperative interaction of *S. pombe* proteins required for mating and morphogenesis. *Cell* **79**, 131–141 (1994).
34. Iwaki, N., Karatsu, K. & Miyamoto, M. Role of guanine nucleotide exchange factors for Rho family GTPases in the regulation of cell morphology and actin cytoskeleton in fission yeast. *Biochem. Biophys. Res. Commun.* **312**, 414–420 (2003).
35. Hampsey, M. A review of phenotypes in *Saccharomyces cerevisiae*. *Yeast* **13**, 1099–1133 (1997).
36. Garton, S., Michaelson, L.V., Beaudoin, F., Beale, M.H. & Napier, J.A. The dihydroceramide desaturase is not essential for cell viability in *Schizosaccharomyces pombe*. *FEBS Lett.* **538**, 192–196 (2003).
37. Takeo, K. *et al.* Rapid, extensive and reversible vacuolation of *Schizosaccharomyces pombe* induced by amphotericin B. *FEMS Microbiol. Lett.* **108**, 265–269 (1993).
38. Piel, J. Bacterial symbionts: prospects for the sustainable production of invertebrate-derived pharmaceuticals. *Curr. Med. Chem.* **13**, 39–50 (2006).
39. Ho, C.H. *et al.* A molecular barcoded yeast ORF library enables mode-of-action analysis of bioactive compounds. *Nat. Biotechnol.* **27**, 369–377 (2009).
40. Bolard, J. How do the polyene macrolide antibiotics affect the cellular membrane properties? *Biochim. Biophys. Acta* **864**, 257–304 (1986).
41. Shogomori, H. & Kobayashi, T. Lysenin: a sphingomyelin specific pore-forming toxin. *Biochim. Biophys. Acta* **1780**, 612–618 (2008).
42. Matsuyama, A. *et al.* pDUAL, a multipurpose, multicopy vector capable of chromosomal integration in fission yeast. *Yeast* **21**, 1289–1305 (2004).
43. Gachet, Y. & Hyams, J.S. Endocytosis in fission yeast is spatially associated with the actin cytoskeleton during polarised cell growth and cytokinesis. *J. Cell Sci.* **118**, 4231–4242 (2005).

Acknowledgments

We thank C. Boone (Univ. Toronto) for sharing unpublished results and discussions, A. Fujie (Astellas Pharma) for kind gifts of FK463 and cispentacin, K. Takegawa (Kyushu Univ.) for *erg* deletion strains, T. Kuno (Kobe Univ.) for the *bgs1* mutant and *pck* deletion strains and K. Nakano (University of Tsukuba) for *rho1*-expression plasmids. We also thank J. Ishiguro (Konan Univ.) for the *act1/cps8* mutant strain, which was provided through the Yeast Genetic Resource Center (YGRC), N. Kanoh, S. Shimizu and H. Osada (RIKEN Advanced Science Institute) for helping in the preparation of TNM affinity beads, J. Ochi (Kyoto Univ.) for technical assistance and J. Piotrowski (RIKEN Advanced Science Institute) for critical reading of the manuscript. We are grateful to the RIKEN Brain Science Institute's Research Resource Center for mass spectrometry. This work was supported in part by the New Energy and Industrial Technology Development Organization Project on Development of Basic Technology to Control Biological Systems Using Chemical Compounds, a Grant-in-Aid from the Ministry of Education, Culture, Sports, Science and Technology of Japan and the Chemical Genomics Research Project, RIKEN Advanced Science Institute.

Author contributions

M.Y. is responsible for project planning and experimental design, with support from K.I., H. Kawasaki, H. Kakeya and T.K.; S.N. performed most of the experiments; Y.A. assisted *in vitro* sterol binding experiments; M.H. assisted chemical-genomic screen; A.M. and A.S. prepared the yeast strain collection; S.M. prepared theonellamides.

Competing financial interests

The authors declare no competing financial interests.

Additional information

Supplementary information, chemical compound information and chemical probe information is available online at http://www.nature.com/naturechemicalbiology/. Reprints and permissions information is available online at http://npg.nature.com/reprintsandpermissions/. Correspondence and requests for materials should be addressed to M.Y.

Lung Cancer xxx (2009) xxx–xxx

Contents lists available at ScienceDirect

Lung Cancer

journal homepage: www.elsevier.com/locate/lungcan

Breast cancer resistant protein (BCRP) is a molecular determinant of the outcome of photodynamic therapy (PDT) for centrally located early lung cancer

Jitsuo Usuda[a,*], Yoshihiko Tsunoda[a], Shuji Ichinose[a], Taichirou Ishizumi[a], Keishi Ohtani[a], Sachio Maehara[a], Shoutarou Ono[a], Hidemitsu Tsutsui[a], Tatsuo Ohira[a], Tetsuya Okunaka[b], Kinya Furukawa[c], Yoshikazu Sugimoto[d], Harubumi Kato[a], Norihiko Ikeda[a]

[a] Department of Thoracic Surgery, Tokyo Medical University, 6-7-1, Nishishinjuku, Shinjuku-ku, Tokyo 160-0023, Japan
[b] Respiratory Disease Center, Sanno Hospital, International University of Health and Welfare, Tokyo 107-0052, Japan
[c] Department of Thoracic Surgery, Tokyo Medical University Kasumigaura Hospital, Kasumigaura, Japan
[d] Keio University, Faulty of Pharmacy, Tokyo, Japan

ARTICLE INFO

Article history:
Received 28 January 2009
Received in revised form 31 March 2009
Accepted 11 April 2009

Keywords:
Photodynamic therapy (PDT)
Lung cancer
Centrally located early lung cancer
Breast cancer resistant protein (BCRP)

ABSTRACT

The ATP-binding cassette (ABC) transporter protein, BCRP (breast cancer resistance protein)/ABCG2 pumps out some types of photosensitizers used in photodynamic therapy (PDT) and causes resistance to the antitumor effect of PDT. The purpose of this study was to investigate the association between the expression of BCRP and the efficacy of PDT using Photofrin, or the second-generation photosensitizer, NPe6, for centrally located early lung cancers.

Using human epidermoid carcinoma cells, A431 cells and the BCRP-overexpressing A431/BCRP cells, we examined the effects of BCRP expression on the effect of PDT by cell viability assay *in vitro*, and investigated the expression of BCRP by immunohistochemical analysis in 81 tumor samples obtained from patients with centrally located early lung cancers.

The A431/BCRP cells were more resistant to Photofrin-PDT than A431 cells *in vitro*, and Fumitremorgin C, a specific inhibitor of BCRP, reversed the resistance.

However, there was no significant difference in the antitumor effect of NPe6-PDT between these cells. All of the 81 centrally located early lung cancer lesions were BCRP-positive (2+, 45 lesions; 1+, 30 lesions) and all the patients were male and heavy smokers (>30 pack-years). The expression of BCRP significantly affected the efficacy of Photofrin-PDT in cancer lesions $\geq$10 mm in diameter ($P = 0.04$). On the other hand, NPe6-PDT exhibited a strong antitumor effect, regardless of the expression status of BCRP.

Photofrin may be a substrate of BCRP and be pumped out from the cells, therefore, BCRP may be a molecular determinant of the outcome of Photofrin-PDT.

1. Introduction

Photodynamic therapy (PDT), used as a treatment modality for many cancers, uses a tumor-specific photosensitizer and laser irradiation to induce the production of reactive oxygen species in cancer cells [1,2]. PDT is widely used as a treatment option for solid cancers and also for some non-cancerous diseases [3]. The first health agency approval for PDT using Photofrin®, the most commonly employed photosensitizer, was obtained in Canada in 1993, and the substance was then approved by the United States Food and Drug Administration (FDA) for the treatment of early stage lung cancer as well as advanced esophageal and lung cancers [1,3].

In Japan, PDT is recommended as a treatment option for centrally located early lung cancers, which are roentgenograhically occult squamous cell carcinomas located no distal to the segmental bronchi, that are histologically determined to be carcinoma *in situ* or carcinoma showing only limited invasion, with no evidence of invasion beyond the bronchial cartilage, as defined in the therapeutic guidelines for lung cancer established by the Japanese Ministry of Health, Labour and Welfare based on the principles of evidence-based medicine [4,5]. Centrally located early lung cancers can be detected in patients at high risk by either sputum cytology or bronchoscopic evaluation [6]. One to 4% of these patients have a synchronous lung cancer, and the risk of a second lung cancer ranges from 1% to 25% per year [7]. For the patients with centrally located early lung cancer, PDT allows preservation of lung function and effective treatment, and is recommended for treatment in the American College of Chest Physician (ACCP) evidence-based clinical practice guidelines [8]. The second-generation photosensitizer,

* Corresponding author. Tel.: +81 3 3342 6111; fax: +81 3 3349 0326.
E-mail address: jusuda@tokyo-med.ac.jp (J. Usuda).

0169-5002/$ – see front matter © 2009 Elsevier Ireland Ltd. All rights reserved.
doi:10.1016/j.lungcan.2009.04.002

talaporfin sodium (NPe6, laserphyrin), which has a major absorption band at 664 nm, was approved by the Japanese government for use in the diagnosis/treatment of centrally located early lung cancer [4,5]. A phase II clinical study using NPe6 and a diode laser for early stage lung cancer demonstrated excellent antitumor effects and safety, including a significantly lower skin incidence of photosensitivity as compared to that observed with photofrin [9]. The Japanese government approved the use of NPe6 for PDT in 2003, and the product has been available in the Japanese market since June 2004 [4,5]. Recently, we established the autofluorescence diagnosis system integrated into a videoendoscope (SAFE-3000) as a very useful technique for the early diagnosis of lung cancer [10]. The novel photodynamic diagnosis (PDD) system using SAFE-3000 and NPe6 improved the quality and efficacy of PDT and avoided misjudgment of the dose of the photosensitizer or laser irradiation in PDT [11]. It has been reported that PDT induces direct tumor cell kill, as well as indirect effects on the tumor microenvironment [12]. PDT rapidly induces apoptosis, inflammatory reactions, tumor-specific and/or—non-specific immune reactions and damage to the microvasculature of the tumor bed [13–15]. Sitnik et al. reported that the microvasculature damage induced by PDT is readily observable histologically and is associated with a significant decrease of the blood flow and severe hypoxia in the tumor [16]. Recently, we examined the role of immunological reactions in the antitumor effects of PDT using cytokine-overexpressing cells [17], and we demonstrated that the extent of photodamage of the anti-apoptotic protein, Bcl-2, caused by PDT determined the sensitivity of cancer cells to apoptosis and the overall cell killing by PDT [18–20]. However, the relationship between the anticancer potency of PDT and the immunological reactions induced by it, is still controversial, and the precise mechanism of the antitumor effect of PDT remains unclear.

Recently, it was reported that the expression of the ATP-binding cassette (ABC) transport proteins renders tumor cells resistant to chemotherapeutic drugs that are substrates of these proteins [21–23], and the effect of these transporters on the intracellular accumulation of photosensitizer has been examined as a potential cause of resistance to PDT [24]. Several members of the ABC transporter protein family may be involved in MDR (multi-drug resistance) in human tumor cells, including P-glycoprotein (Pgp), MDR protein (MRP)1, MRP2, and MRP3 [20]. Elevated expression of breast cancer resistant protein (BCRP) in particular, also known as ABCG2, has been shown to cause resistance to anticancer drugs *in vitro*, including to topotecan, irinotecan, mitoxantrone and doxorubicin [21,22]. Robey et al. reported that BCRP transported some photosensitizers out of cells to decrease intracellular photosensitizer accumulation, suggesting that the presence of BCRP might be a possible cause for cellular resistance to PDT [24]. Jonker et al. also showed that BCRP-knockout mice were photosensitive because of increased intracellular protoporphyrin IX (PpIX) levels [25].

In this study, we examined the association between the expression of BCRP and the efficacy of PDT by retrospectively examining the expression levels of BCRP in clinical samples of centrally located early lung cancers, and investigated whether BCRP expression might be a determinant of the outcome of PDT in lung cancers.

2. Material and methods

2.1. Cell culture

A431 human epidermoid carcinoma cells were cultured in Dulbecco's modified Eagle's medium (DMEM) supplemented with 10% fetal bovine serum at 37 °C in 5% CO_2 [22]. A431/BCRP cells were established by the transduction of A431 cells with a HaBCRP retrovirus vector composed of Myc-tagged human BCRP cDNA in the Ha retrovirus vector [22,26]. The stably transfected cell line was maintained in the drug-free medium for up to 3 months.

2.2. Photosensitizer

Photofrin (Wyeth Japan K.K., Tokyo, Japan), a hydrophobic hematoporphyrin derivative, remains in a complex mixture with inherent variability, and has been shown to exhibit strong tumor affinity [5,11,17,20]. It is activated by a highly transmissive red light having a wavelength of 630 nm, to produces a photochemical reaction [4,5,20]. NPe6 (Meiji Seika, Tokyo, Japan) is a second-generation water-soluble photosensitizer with a molecular weight of 799.69 and a chlorine annulus, and has its highest absorption peak at the wavelengths of 407 nm and a second peak at the wavelength of 664 nm. NPe6 exhibits superior in tumor affinity as compared to Photofrin, and is excited by visible red light with a longer wavelength of 664 nm, which allows deeper and better penetration into living tissues [4,5,11,20].

2.3. Laser unit

An excimer dye laser (Hamamatsu Photonics K.K., Hamamatsu, Japan) emitting pulse-wave laser light at a wavelength of 630 nm was used as the light source for the excitation of Photofrin [4,5]. A diode laser (Matsushita Electric Industrial Co., Osaka, Japan) emitting continuous-wave laser light at a wavelength of 664 nm was used as the light source for the excitation of NPe6 [4,5,11].

2.4. Measurement of the fluorescence intensity of Photofrin and NPe6 in the cells

Cells were exposed to Photofrin (2.5 μg/ml) or NPe6 (15 μg/ml) for 4 h and washed with phosphate-buffered saline (PBS). The photosensitizers were used at the IC_{50} dose. The photosensitizer in the cells was excited at 405 nm, and the fluorescence was detected with a charge-coupled device (CCD) camera system (Argus/Hisca, Hamamatsu Photonics Co. Ltd., Hamamatsu, Japan) through a multilaminate interference filter that can select the fluorescence wavelength at 630 as previous report [27].

2.5. Determination of the cell viability

Cells were seeded into 96-well microculture plates at 1×10^4 cells/well and allowed to adhere to the dish overnight. The medium was removed and replaced with that containing or not containing a specific inhibitor of BCRP inhibitor, Fumitremorgin C (FTC) (Alex biochemical Inc., CA, USA) [24,26,28]. Fifteen minutes later, the photosensitizer (Photofrin or NPe6) was added to the cells in increasing concentrations, followed by incubation at 37 °C in the dark for 4 h. The cells were washed with PBS and incubated with 10% FBS-DMEM for 1 h, and then washed again with PBS and irradiated with laser (33 mW/cm^2, total energy 10 J/cm^2) [27], followed by incubation for an additional 24 h. Cell viability was measured using the tetrazolium salt WST-1 assay, in accordance with the manufacturer's instructions [27,29]. Independent experiments were repeated at least three times to confirm the data.

2.6. Criteria for the diagnosis of centrally located early lung cancer

Lung cancers located no distal to segmental bronchi, diagnosed histologically as squamous cell carcinoma and determined to be carcinoma *in situ* or carcinoma showing only limited invasion with no evidence of invasion beyond the bronchial cartilage were defined as centrally located early lung cancers, which are roentgenographically occult [4,5,11]. We routinely determined the tumor depth

Please cite this article in press as: Usuda J, et al. Breast cancer resistant protein (BCRP) is a molecular determinant of the outcome of photodynamic therapy (PDT) for centrally located early lung cancer. Lung Cancer (2009), doi:10.1016/j.lungcan.2009.04.002

by EBUS (endobronchial ultrasonography), and it was confirmed that the tumors did not invade the bronchial wall beyond the level of the carlitage and that they were confined to the basal membrane of the mucosa, submucosa or intracarlitagious layers of the bronchial wall [4,5,11]. In 2003, the Japan Photodynamic Association and Japanese Society of Laser Surgery and Medicine established the following therapeutic criteria for PDT in cases with centrally located early lung cancers [4,5,11]: patients with [1] endoscopically assessable early lung cancer [2], normal chest X-ray and CT (roentgenographically occult) [3], no metastasis to lymph nodes or distant metastasis as revealed by routine clinical diagnostic methods, including fluorodeoxyglucose-position emission tomography (FDG-PET) for staging.

2.7. Procedures of PDT and follow-up

PDT was performed using Photofrin or NPe6. Laser irradiation (630 nm) for Photofrin-PDT was transmitted via quartz fibers inserted through the biopsy channel of the endoscope, 48 h after the administration of the photosensitizer, Photofrin (2 mg/kg). On the other hand, for NPe6-PDT, laser irradiation was accomplished 4 h after the administration of NPe6 using a diode laser, the PD laser (40 mg/m^2). The total energy of the laser irradiation was: 100 J/cm^2, 150 mW/cm^2 [4,5,9,11].

The Japanese government approved the use of NPe6 for PDT against centrally located early lung cancers in 2003, and the product became available in the Japanese market in June 2004 [4,5,11]. Ever since, we have used NPe6 for PDT. Fiberoptic bronchoscopy with cytological and histological examination was performed at 1, 2 and 3 months after the PDT, and thereafter, at 3-month intervals during the first year and 6-month intervals during the second year after PDT. The antitumor effect of the initial treatment was rated based on endoscopic measurement of the tumor size using forceps, the morphologic appearance, and the pathological findings of the biopsy specimens, in accordance with the general rules of the Japan Lung Cancer Society and the Japan Society of Clinical Oncology [4,5,11]. The antitumor effect was again evaluated at 3 months after the PDT. The tumors were then classified as showing complete response (CR) (no microscopically demonstrable tumor in the brushings and or biopsy specimens over a period of 4 weeks) [5,9,11].

2.8. Patient selection

A total of 110 patients (128 lesions) with centrally located early lung cancer received PDT at the Tokyo Medical University Hospital between January 1998 and December 2006. Adequate tumor biopsy specimens were obtained from 81 of these lesions (57 from the Photfrin-PDT group and 24 from the NPe6-PDT group, and the specimens were analyzed retrospectively in this study. The clinicopathological characteristics of the patients are listed in Table 1. Their median age at diagnosis was 71 years (range, 56–84). All the patients were male and heavy smokers with a smoking history of >30 pack-years. All of the lesions were diagnosed as squamous cell carcinoma. PDT and tumor biopsy were undertaken in the patients after obtaining their informed consent in accordance with the institutional guidelines, on the basis of the criteria for PDT criteria, all of patients underwent tumor biopsy and PDT.

2.9. Immunohistochemical analysis

Immunohistochemical staining was performed on 4 μM formalin-fixed, paraffin-embedded tissue sections [31]. The slides were deparaffinized in xylene and dehydrated in a graded ethanol series. Endogenous peroxidase was blocked with 0.3% H_2O_2 in methanol for 10 min. All of the slides were heated to 95 °C by exposure to microwave irradiation for 20 min. The slides were then cooled for 1 h at room temperature and washed in PBS. Non-specific binding was blocked by preincubation with 1% BSA for 30 min. After washing with PBS, the slides were incubated for 1 h at room temperature with anti-BCRP antibody (Bxp-21; Chemicon, Temecula, CA, USA) [22,26,30–34]. Staining with the antibodies was considered to be positive if ≥10% of the tumor cells were stained, based on the use of the 10% cutoff level in several previous studies [31,33,34]. All of the slides were examined and scored independently by two observes without knowledge of the patient clinical data.

Table 1
Characteristics of centrally located early lung cancer (January 1998–December 2006).

Characteristics	Number of lesions
Patients (lesions)	79 (81)
Age	67–83
Gender	Male: 79 Female: 0
Histology	Sq. cell ca.: 81 lesions
Smoking history	Positive: 79 (>30 pack-years) Negative: 0
PDT	
Photofrin:	57 lesions
NPe6:	24 lesions

The immunohistochemical staining was scored based on the estimated average staining intensity of the tumor cells: (−), negative; (+), intermediate; and (2+), strongly positive [35,36]. This study was conducted with the approval of the Ethical Committee of Tokyo Medical University.

2.10. Statistical analysis

The correlations between immunohistochemical expression and the clinical variables and response to Photofrin-PDT were evaluated by χ^2-test or Fisher's exact test when required; p-values of less than 0.05 were considered to be significant [31,37].

3. Results

3.1. Cellular accumulation of the photosensitizers Photofrin and NPe6 in the A431 cells and A431/BCRP cells

We examined the cellular accumulation of Photofrin and NPe6 in the A431 cells and A431/BCRP cells based on the fluorescence intensities, because photosensitizer accumulation has been considered as a factor influencing the cellular sensitivity to PDT [2,19,20]. As reported previously, Photofrin localized not only to the mitochondria, but also to the endoplasmic reticulum (ER), Golgi complexes and possibly other intracellular organelles (Fig. 1A). NPe6 localized not only to the lysosomes, but also to the ER (Fig. 1A) [20]. The photosensitizers did not localize to the plasma membrane or the nucleus, which was consistent with previous reports [18–20]. We analyzed the fluorescence intensity of the red fluorescence of Photofrin or NPe6. The fluorescence intensity of Photofrin was significantly higher in the A431 cells than in the A431/BCRP cells (Fig. 1B). The fluorescence intensity of Photofrin decreased in A431/BCRP cells in the presence of a specific inhibitor of BCRP, Fumitremorgin C (data not shown). However, there was no difference of the fluorescence intensity of NPe6 between the A431 cells and A431/BCRP cells (Fig. 1B). These results suggest that while BCRP was able to pump out Photofrin from the cells, but not NPe6, and that Photofrin may thus be a substrate of BCRP.

Please cite this article in press as: Usuda J, et al. Breast cancer resistant protein (BCRP) is a molecular determinant of the outcome of photodynamic therapy (PDT) for centrally located early lung cancer. Lung Cancer (2009), doi:10.1016/j.lungcan.2009.04.002

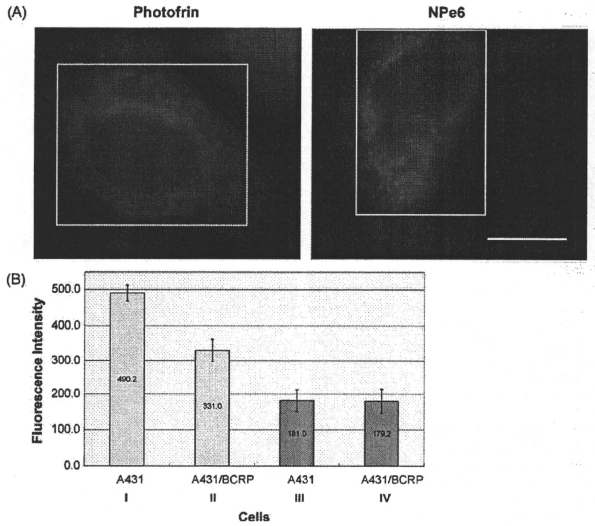

Fig. 1. (A) Localization of Photofrin and NPe6 in A431 cells. Cells were exposed to 2.5 μg/ml Photofrin (A) and 15 μg/ml NPe6 (B) for 4 h and then washed. The photosensitizers were used at the IC_{50} dose. The Photofrin or NPe6 in the cells was excited at 405 nm and the fluorescence was detected using a CCD camera system. *Scale bar*, 5 μm. (B) The fluorescence intensity per cell. We counted the fluorescence intensity of 10 cells and showed the average intensity per cell. The fluorescence of Photofrin in the A431 cells (i) and A431/BCRP cells (ii), and the fluorescence of NPe6 in the A431 cells (iii) and A431/BCRP cells (iv). There was a significant difference in the intensity of Photofrin between the A431 and A431/BCRP cells ($P < 0.05$).

3.2. Growth-inhibitory effect of Photofrin-PDT and NPe6-PDT on BCRP-overexpressing cells

We evaluated the antitumor effect of Photofrin-PDT and NPe6-PDT on the BCRP-overexpressing A431/BCRP cells by the WST assay [28,29]. The survival curves indicate that the A431/BCRP cells were comparatively resistant as compared to the parental A431 cells to Photofrin-PDT (Fig. 2A). At the 50% survival level, the presence of BCRP provided a dose-modifying factor of 1.86. Moreover, Fumitremorgin C, a specific inhibitor of BCRP, reversed the resistance of the A431/BCRP cells to Photofrin-PDT (Fig. 2A). These results suggest that Photofrin, a photosensitizer for PDT, may be transported out of the cells by BCRP and that BCRP expression may cause resistance to Photofrin-PDT. The survival curves indicate that, on the other hand, there was no significant difference in the antitumor effect of NPe6-PDT between the A431/BCRP cells and the parent A431 cells (Fig. 2B). This result suggests that NPe6 is not a substrate of BCRP and that BCRP expression does not exert any significant regulatory effect on the cell survival in NPe6-PDT. These results indicate that BCRP is a molecular determinant of resistance to Photofrin-PDT, but not to NPe6-PDT.

3.3. Expression of BCRP in centrally located early lung cancers

Previously we examined the immunohistochemical analysis of BCRP expression in A431 and A431/BCRP cells. We observed the negative expression of BCRP on A431 cells using anti-BCRP antibody, Bxp-21 [30]. Representative immunohistochemical BCRP staining is shown in Fig. 3A–C. It has been reported that BCRP is expressed in the normal small intestine, colon, liver, and mammary gland of the breast but is quite a low level in the lung [31,32]. In Fig. 3, the immunostaining of BCRP was both membranous and cytoplasmic as previous reports (Fig. 3) [33,34]. All of the 81 cancer lesions were BCRP-positive and were examined and scored according to the intensity of staining as compared with that in the negative control (+, positive; 2+, strong positive) independently by two observers [35,36]. In Fig. 3A and B, carcinoma cells showed strong positive reaction (2+) to anti-BCRP antibody, whereas in Fig. 3C and D, they showed positive reaction (1+).

3.4. Relationship between the expression of BCRP and the efficacy of PDT

Evaluation of the efficacy of PDT is shown in Table 2. The complete response rate of the centrally located early lung cancer lesions to Photofrin-PDT was 73.6% (42/57 lesions, BCRP(+); 24 lesions, BCRP(2+); 18 lesions). Of the 57 lesions, the remaining 15 showed PR or recurrence after CR (BCRP(+); 6 lesions, BCRP(2+); 9 lesions). As shown in Tables 3 and 4, 25 lesions were <1.0 cm in diameter and

Table 2
Relationship between expression of BCRP and response to Photofrin-PDT ($n = 57$).

PF-PDT	Lesions	BCRP		
		(−)	(1+)	(2+)
CR	42	0	24	18
[a]Rec, PR	15	0	6	9
CR rate	736.6%		80.0%	66.7%

[a] Rec, recurrence.

Please cite this article in press as: Usuda J, et al. Breast cancer resistant protein (BCRP) is a molecular determinant of the outcome of photodynamic therapy (PDT) for centrally located early lung cancer. Lung Cancer (2009), doi:10.1016/j.lungcan.2009.04.002

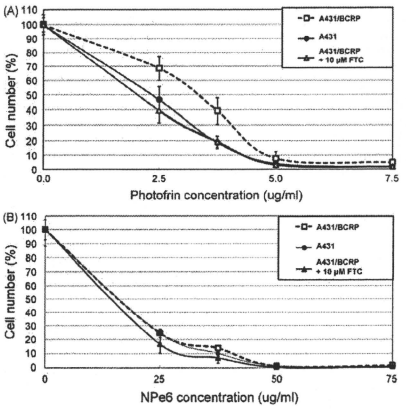

Fig. 2. (A) Growth-inhibitory effect of Photofrin-PDT in A431 cells (●), A431/BCRP cells (□) and A431/BCRP cells in the presence of Fumitremorgin C (△). Cells were exposed to Photofrin (0, 2.5, 3.75, 5, 10 μg/ml) for 4 h and then washed twice and incubated in fresh medium containing or not containing 10 μM FTC for 1 h, followed by laser-irradiation (664 nm) at 10 J/cm². The growth-inhibitory effect was measured 24 h after the PDT by WST assay. (B) Growth-inhibitory effect of NPe6-PDT in A431 cells (●), A431/BCRP cells (□) and A431/BCRP cells in the presence of Fumitremorgin C (▲). Cells were exposed to Photofrin (0, 25, 37.5, 50, 75 μg/ml) for 4 h and then washed twice and incubated in fresh medium containing or not containing 10 μM FTC for 1 h, followed by laser-irradiation (664 nm) at 10 J/cm². The growth-inhibitory effect was measured 24 h after the PDT by WST assay.

32 were ≥1.0 cm in diameter prior to the PDT, showing CR rates of 92% (23/25) and 59% (19/32), respectively (significant difference). As shown in Table 3, there was no difference of CR rate between BCRP(1+) and BCRP(2+) in tumor lesions <1.0 cm. Especially, among

Table 3
Relationship between expression of BCRP and response to Photofrin-PDT in tumor lesion (<1.0 cm) ($n = 25$).

Size <1.0 cm	Lesions	BCRP		
		(−)	(1+)	(2+)
CR	23	0	10	13
[a]Rec, PR	2	0	1	1
CR rate	92.0%		90.9%	92.9%

[a] Rec, recurrence.

Table 4
Relationship between expression of BCRP and response to Photofrin-PDT in tumor lesion (≥1.0 cm) ($n = 32$).

Size ≥1.0 cm	Lesions	BCRP		
		(−)	(1+)	(2+)
CR	19	0	14	5
[a]Rec, PR	13	0	5	8
CR rate	59.3%		73.7%[b]	38.5%[c]

[a] Rec, recurrence.
[b,c] Statistically significant difference of CR rate between BCRP (1+) and BCRP (2+) ($P < 0.05$).

lesions ≥1.0 cm in diameter, eight lesions that showed recurrence or only PR were BCRP(2+) and 5 lesions were BCRP(+). The efficacy with a significant difference of CR rate was seen in lesions with BCRP(2+) (38.5%) compared to lesions with BCRP(1+) (73.7%) (Table 4). These results, in particular, indicate that the expression of BCRP can significantly affect the efficacy of Photofrin-PDT for lesions ≥1.0 cm (Fisher's exact test; $P = 0.04$). On the other hand, as shown in Table 5 the CR rate of the lesions to NPe6-PDT was 91.6% (22/24 lesions), and much higher as compared with that to Photofrin-PDT (73.6%). Of these 24 lesions for which NPe6-PDT was undertaken, there were 2 BCRP(+) cases that showed PR. All the remaining 22 lesions were BCRP(1+) or strongly positive for BCRP(2+). NPe6-PDT achieved CR in all 18 lesions with BCRP(2+), the CR rate was 100%. These data suggest that NPe6-PDT exerted strong

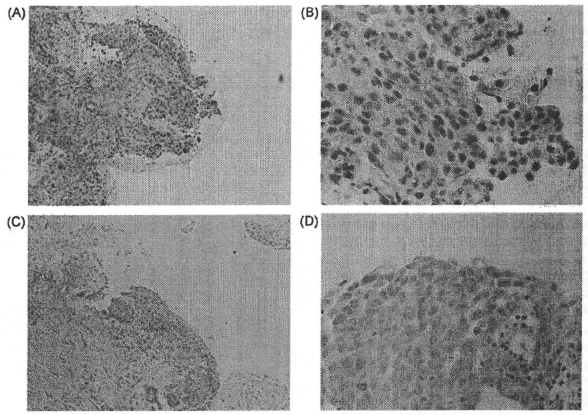

Fig. 3. Immunohistochemical staining of centrally located early lung cancers with anti-BCRP antibody (Bxp-21). The immunohistochemical staining was scored based on the estimated average staining intensity as strongly positive (2±) (A, ×40; B, ×400) and intermediate (1±) (C, ×40; D, ×400).

Please cite this article in press as: Usuda J, et al. Breast cancer resistant protein (BCRP) is a molecular determinant of the outcome of photodynamic therapy (PDT) for centrally located early lung cancer. Lung Cancer (2009), doi:10.1016/j.lungcan.2009.04.002

Table 5
Relationship between expression of BCRP and response to NPe6-PDT ($n = 24$).

NPe6-PDT	Lesion	BCRP		
		(−)	(1+)	(2+)
CR	22	0	4	18
[a]Rec, PR	2	0	2	0
CR rate	91.6%		66.7%	100%

[a] Rec, recurrence.

antitumor effect, regardless of the BCRP expression, and especially among lesions ≥10 mm in diameter (data not shown), the CR rate to NPe6-PDT was much higher than that to Photofrn-PDT.

4. Discussion

In this study, using the WST assay as the sensitivity test, we showed that BCRP-overexpressing cells were resistant to Photofrin-PDT as compared to the parental cells *in vitro* (Fig. 2A); we also showed, based on analysis of the treatment outcome of centrally located early lung cancers, that BCRP expression affected the efficacy of Photofrin-PDT (Table 2). We hypothesized that Photofrin may be a substrate of BCRP, which is a member of the ABC transporter protein family. *In* Fig. 1A and B, we examined the accumulation of the photosensitizers, Photofrin and NPe6, based on detection of the fluorescence intensity by fluorescence microscopy, and showed less pronounced accumulation of Photofrin in the A431/BCRP cells than in the parental A431 cells. Treatment with the specific inhibitor of BCRP, Fumitremorgin C, reversed the resistance against Photofrin-PDT in the A431/BCRP cells. We therefore hypothesized that Photofrin may be a substrate of BCRP. However, recently Liu et al. reported that Photofrin was minimally transported [38], and speculated that Photofrin is a mixture of multimeric photosensitizers that are considered to be clinically active fractions, together with monomers that are poorly retained in the cells and tissues and have little biological efficacy, and that only these inactive monomers are BCRP substrates [38]. It still remains under debate as to whether or not Photofrin is a substrate of BCRP. From our analysis of the BCRP expression in centrally located early lung cancers, we concluded that the expression of BCRP significantly affected the efficacy of Photofrin-PDT, and that BCRP could be a molecular determinant of the outcome of Photofrin-PDT.

On the other hand, as shown in Fig. 2B, in the case of NPe6-PDT, there was no significant difference in the sensitivity between A431 cells and A431/BCRP cells, and treatment with the specific inhibitor of BCRP, Fumutremorgin C, did not affect the sensitivity. Robey et al. reported that BCRP-overexpressing cells were not resistant to PDT with meso-tetra-3-hydroxyphenyl chlorine (m-THPC), which has a similar structure to the NPe6 chlorine annulus [24]. We concluded that NPe6 is not a substrate of BCRP and does not therefore affect the sensitivity of PDT.

In this study, all of the 81 centrally located lung lesions were found to express BCRP. Yoh et al. reported that 46% of all lung cancers were BCRP-positive in particular, 39% of squamous cell lung cancers [31]. Our data showed that all of the patients with centrally located early lung cancers were male, heavy smokers (>30 pack-years), and all of the tumors were BCRP-positive (100%). We hypothesized that smoking induces the expression of BCRP, and that some chemical products may act as substrates of BCRP. Recently, cigarette smoking was found to significantly lower both the exposure to irinotecan, which is a topoisomerase I inhibitor and a substrate of BCRP, and treatment-induced neutropenia, with a potential risk of treatment failure [39]. In addition, induction of ABC transporters by smoking can result in the elimination of irinotecan and its metabolites, suggesting that cigarette smoking may influence the pharmacokinetics of irinotecan via modulation of the ABC transporters [40,41]. Kolwankar et al. reported, based on immunohistochemical analysis of 94 patients with non-small cell lung carcinoma higher expression levels of ABCB1 (P-glycoprotein, MRP1) in smokers (58% vs. 9%; $P < 0.01$) [42]. In our study, we also examined the association between the efficacy of PDT and the expression of other ABC transporters, namely, MDR1/P-gp, MRP1/ABCC1. A431/MDR1 cells and KB3-1/MRP1 cells were slightly resistant to Photofrin-PDT as compared to the parental cells [30]. From analysis of the dose-modifying factor at the IC_{50} using these three cell lines, we suspect that BCRP may play the most important role among the three ABC transporters in influencing the outcome of clinical PDT. Although the data were not sufficient to arrive at any definitive conclusion in regard to the influence of smoking on the ABC transporters, we conclude that there may be some associations between the expression of the ABC transporters and smoking, and that BCRP, in particular, affected the efficacy of Photofrin-PDT. Additional investigation may be required to determine the mechanism underlying these results, and the expression of BCRP in centrally located early lung cancers may have important clinical implications.

For the treatment of centrally located early lung cancers, NPe6-PDT would appear to be superior to Photofrin-PDT, because the expression of BCRP did not seem to affect the antitumor effect of NPe6-PDT. Recently, it has been reported that the tyrosine kinase inhibitor imatinib mesylate (Gleevec) can block the functions of BCRP, to increase the intracellular accumulation of photosensitizers such as protoprphyrin IX (PpIX), in BCRP-overexpressing tumors [38]. Many advanced cancers have elevated expression levels of the BCRP protein and we hypothesize that PDT combined with administration of BCRP inhibitors such as imatinib can overcome any resistance conferred by elevated expression amounts of BCRP. In conclusion, for the treatment of centrally located early lung cancers with high expression levels of BCRP, NPe6-PDT would appear to be better than Photodrin-PDT, and individualized treatment based on the expression status of BCRP may improve the efficacy of PDT in patients with lung cancer.

Conflict of interest statement

None declared.

Acknowledgement

This study was supported in part by a Grant-in-Aid for Japan Society for the Promotion of Science (JSPS) Fujita Memorial Fund for Medical Research (to J.U.).

References

[1] Dougherty TJ, Gomer CJ, Henderson BW, Jori G, Kessel D, Korbelik M, et al. Photodynamic therapy. J Natl Cancer Inst 1998;90:889–905.
[2] Oleinick NL, Morris RL, Belichenko I. The role of apoptosis in response to photodynamic therapy: what, where, why, and how. Photochem Photobiol Sci 2001;1:1–21.
[3] Dougherty TJ. An update on photodynamic therapy applications. J Clin Laser Med Surg 2002;20:3–7.
[4] Kato H, Usuda J, Okunaka T, Furukawa K, Honda H, Sakaniwa N, et al. Basic and clinical research on photodynamic therapy at Tokyo Medical University Hospital. Lasers Surg Med 2006;38:371–5.
[5] Usuda J, Kato H, Okunaka T, Furukawa K, Tsutsui H, Yamada K, et al. Photodynamic therapy for lung cancers. J Thorac Oncol 2006;1:489–95.
[6] Lam S, Standish B, Baldwin C, McWilliams A, leRiche J, Gazdar A, et al. *In vivo* optical coherence tomography imaging of preinvasive bronchial lesions. Clin Cancer Res 2008;14:2006–11.
[7] Breuer RH, Pasic A, Smit EF, Vliet E, Noordegraaf AV, Risse EJ, et al. The natural course of preneoplastic lesions in bronchial epithelium. Clin Cancer Res 2005;11:537–43.
[8] Kennedy TC, McWilliams A, Edell E, Sutedja TG, Downie G, Yung R, et al. Bronchial intraepithelial neoplasia/early central airways lung cancer: ACCP evidence-based clinical practice guidelines (2nd edition). Chest 2007;132:221–33.

Please cite this article in press as: Usuda J, et al. Breast cancer resistant protein (BCRP) is a molecular determinant of the outcome of photodynamic therapy (PDT) for centrally located early lung cancer. Lung Cancer (2009), doi:10.1016/j.lungcan.2009.04.002

[9] Kato H, Furukawa K, Sato M, Okunaka T, Kusunoki Y, Kawahara M, et al. Phase II clinical study of photodynamic therapy using mono-L-aspartyl chlorine e6 and diode laser for early superficial squamous cell carcinoma of the lung. Lung Cancer 2003;42:103–11.
[10] Ikeda N, Honda H, Hayashi A, Usuda J, Kato Y, Tsuboi M, et al. Early detection of bronchial lesions using newly developed videoendoscopy-based autofluorescence bronchoscopy. Lung Cancer 2006;52:21–7.
[11] Usuda J, Tsutsui H, Honda H, Ichinose S, Ishizumi T, Hirata T, et al. Photodynamic therapy for lung cancers based on novel photodynamic diagnosis using talaporfin sodium (NPe6) and autofluorescence bronchoscopy. Lung Cancer 2007;58:317–23.
[12] Gomer CJ, Ferrario A, Luna M, Rucker N, Wong S. Photodynamic therapy: combined modality approaches targeting the tumor microenvironment. Lasers Surg Med 2006;38:516–21.
[13] Ferrario A, von Tiehil KF, Rucker N, Schwartz MA, Gill PS, Gomer CJ. Antiangiogenic treatment enhances photodynamic therapy responsiveness in a mouse mammary carcinoma. Cancer Res 2000;60:4066–9.
[14] Korbelik M. PDT-associated host response and its role in the therapy outcome. Lasers Surg Med 2006;38:500–8.
[15] Gollnick SO, Owczarczak B, Maier P. Photodynamic therapy and anti-tumor immunity. Lasers Surg Med 2006;38:509–15.
[16] Sitnik TM, Hampton JA, Henderson BW. Reduction of tumor oxygenation during and after photodynamic therapy *in vivo*: effect of fluence rate. Br J Cancer 1998;77:1386–94.
[17] Ohtani K, Usuda J, Ichinose S, Ishizumi T, Hirata T, Inoue T, et al. High expression of Gadd-45 alpha via upregulation of IL-2 after photodynamic therapy using NPe6. Int J Oncol 2008;32:397–403.
[18] Usuda J, Chiu SM, Murphy ES, Lam M, Nieminen AL, Oleinick NL. Domain-dependent photodamage to Bcl-2: a membrane anchorage region is needed to form the target of phthalocyanine photosensitization. J Biol Chem 2003;278:2021–9.
[19] Usuda J, Azizuddin K, Chiu SM, Oleinick NL. Association between the photodynamic loss of Bcl-2 and the sensitivity to apoptosis caused by phthalocyanine photodynamic therapy. Photochem Photobiol 2003;78:1–8.
[20] Usuda J, Hirata T, Ichinose S, Ishizumi T, Inoue T, Ohtani K, et al. Tailor-made approach to photodynamic therapy in the treatment of cancer based on Bcl-2 photodamage. Int J Oncol 2008;33:689–96.
[21] Izuquierdo MA, van der Zee AG, Vermorken JB, Van Der Valk P, Belien JA, Giaccone G, et al. Drug resistance-associated marker Lrp for prediction of response to chemotherapy and prognoses in advanced ovarian carcinoma. J Natl Cancer Inst 1995;87:1230–7.
[22] Sugimoto Y, Tsukahara S, Ishikawa E, Mitsuhashi J. Breast cancer resistance protein: molecular target for anticancer drug resistance and pharmacokinetics/pharmacodynamics. Cancer Sci 2005;96:457–65.
[23] Ifergan I, Scheffer GL, Assaraf YG. Novel extracellular vesicles mediate an ABCG2-dependent anticancer drug sequestration and resistance. Cancer Res 2005;65:10952–8.
[24] Robey RW, Steadman K, Polgar O, Bates SE. ABCG2-mediated transport of photosensitizers. Cancer Biol Ther 2005;4:187–94.
[25] Jonker JW, Buitelaar M, Wagenaar E, Van Der Valk MA, Scheffer GL, Scheper RJ, et al. The breast cancer resistance protein protects against a major chlorophyll-derived dietary phototoxin and protoporphyria. Proc Natl Acad Sci USA 2002;99:15649–54.
[26] Yanase K, Tsukahara S, Asada S, Ishikawa E, Imai Y, Sugimoto Y. Gefitinib reverses breast cancer resistance protein-mediated drug resistance. Mol Cancer Threapeut 2004;3:1119–25.
[27] Usuda J, Okunaka T, Furukawa K, Tsuchida A, Kuroiwa Y, Ohe Y, et al. Increased cytotoxic effects of photodynamic therapy in IL-6 gene transfected cells via enhanced apoptosis. Int J Cancer 2001;93:475–80.
[28] Nakanishi T, Shiozawa K, Hassel BA, Ross DD. Complex interaction of BCRP/ABCG2 and imatinib in BCR-ABL-expressing cells: BCRP-mediated resistance to imatinib is attenuated by imatinib-induced reduction of BCRP expression. Blood 2006;108:678–84.
[29] Xue LY, Chiu SM, Oleinick NL. Photodynamic therapy-induced death of MCF-7 human breast cancer cells: a role for caspase-3 in the late steps of apoptosis but not for the critical lethal event. Exp Cell Res 2001;263:145–55.
[30] Tsunoda Y, Usuda J, Imai K, Kubota M, Maehara S, Ohtani K, et al. The expression of BCRP/ABCG2 causes resistance to Photofrin-PDT. Jpn J Laser Surg Med 2008;28:355–61.
[31] Yoh K, Ishii G, Yokose T, Minegishi Y, Tsuta K, Goto K, et al. Breast cancer resistance protein impacts clinical outcome in platinum-based chemotherapy for advanced non-small cell lung cancer. Clin Cancer Res 2004;10:1691–7.
[32] Diestra JE, Scheffer GL, Catala I, Maliepaard M, Schellens JH, Scheper RJ, et al. A frequent expression of the multi-drug resistance-associated protein BCRP/MXR/ABCP/ABCG2 in human tumors detected by the BXP-21 monoclonal antibody in paraffin-embedded material. J Pathol 2002;198:213–9.
[33] Filipits M, Haddad V, Schmid K, Huynh A, Dunant A, Andre F, et al. Multidrug resistance proteins do not predict benefit of adjuvant chemotherapy in patients with completely resected non-small cell lung cancer: international adjuvant lung cancer trial biologic program. Clin Cancer Res 2007;13:3892–8.
[34] Kim YH, Ishii G, Goto K, Ota S, Kubota K, Murata Y, et al. Expression of breast cancer resistance protein is associated with a poor clinical outcome in patients with small-cell lung cancer. Lung Cancer, in press, doi:10.1016/j.lungcan.2008.10.008.
[35] Elledge RM, Clark GC, Fuqua SAW, Yu YY, Allred DC. p53 protein accumulation detected by five different antibodies: Relationship to prognosis and heat shock protein 70 in breast cancer. Cancer Res 1994;54:3752–7.
[36] Pollack A, Cowen D, Troncoso P, Zagars GK, von Eschenbach AC, Meistrich ML, et al. Molecular markers of outcome after radiotherapy in patients with prostate carcinoma. Cancer 2003;97:1630–8.
[37] Salaun M, Sesboue R, Moreno-Swirc S, Metayer J, Bota S, Bourguignon J, et al. Molecular predictive factors for progression of high-grade preinvasive bronchial lesions. Am J Respir Crit Care Med 2008;177:880–6.
[38] Liu W, Baer MR, Bowman MJ, Pera P, Zheng X, Morgan J, et al. The tyrosine kinase inhibitor imatinib mesylate enhances the efficacy of photodynamic therapy by inhibiting ABCG2. Clin Cancer Res 2007;13:2463–70.
[39] Van der Bol JM, Mathijssen RH, Loos WJ, Friberg LE, van Schaik RH, de Jonge MJ, et al. Cigarette smoking and irinotecan treatment: Pharmacokinetic interaction and effects on neutropenia. J Clin Oncol 2007;25:2719–26.
[40] De Jong FA, de Jonge MJ, Verweij J, Mathijssen RH. Role of pharmacogenetics in irinotecan therapy. Cancer Lett 2006;234:90–106.
[41] Volm M, Mattern J, Samsel B. Overexpression of P-glycoprotein and glutathione S-transferase-pi in resistant non-small cell lung carcinomas of smoker. Br J Cancer 1991;64:700–4.
[42] Kolwanker D, Glover DD, Ware JA, Tracy TS. Expression and function of ABCB1 and ABCG2 in human placental tissue. Drug Metab Dispos 2005;33:524–9.

Please cite this article in press as: Usuda J, et al. Breast cancer resistant protein (BCRP) is a molecular determinant of the outcome of photodynamic therapy (PDT) for centrally located early lung cancer. Lung Cancer (2009), doi:10.1016/j.lungcan.2009.04.002

Pharmacological interaction with sunitinib is abolished by a germ-line mutation (1291T>C) of *BCRP/ABCG2* gene

Haruka Kawahara, Kohji Noguchi, Kazuhiro Katayama, Junko Mitsuhashi and Yoshikazu Sugimoto[1]

Division of Chemotherapy, Faculty of Pharmacy, Keio University, Tokyo, Japan

(Received December 25, 2009/Revised February 8, 2010/Accepted February 12, 2010/Accepted manuscript online February 22, 2010/Article first published online March 19, 2010)

Sunitinib malate (Sutent, SU11248) is a small-molecule multitargeted tyrosine kinase inhibitor (TKI) used for the treatment of renal cell carcinoma and imatinib-resistant gastrointestinal stromal tumors. Some TKIs can overcome multidrug resistance conferred by ATP-binding cassette transporter, P-glycoprotein (P-gp)/ABCB1, multidrug resistance-associated protein 1 (MRP1)/ABCC1, and breast cancer resistance protein (BCRP)/ABCG2. Here, we analyzed the effects of sunitinib on P-gp and on wild-type and germ-line mutant BCRPs. Sunitinib remarkably reversed BCRP-mediated and partially reversed P-gp-mediated drug resistance in the respective transfectants. The *in vitro* vesicle transport assay indicated that sunitinib competitively inhibited BCRP-mediated estrone 3-sulfate transport and P-gp-mediated vincristine transport. These inhibitory effects of sunitinib were further analyzed in Q141K-, R482G-, R482S-, and F431L-variant BCRPs. Intriguingly, the F431L-variant BCRP, which is expressed by a germ-line mutant allele 1291T>C, was almost insensitive to both sunitinib- and fumitremorgin C (FTC)-mediated inhibition in a cell proliferation assay. Sunitinib and FTC did not inhibit ^{125}I-iodoarylazidoprazosin-binding to F431L-BCRP. Thus, residue Phe-431 of BCRP is important for the pharmacological interaction with sunitinib and FTC. Collectively, this is the first report showing a differential effect of a germ-line variation of the *BCRP/ABCG2* gene on the pharmacological interaction between small-molecule TKIs and BCRP. These findings would be useful for improving our understanding of the pharmaceutical effects of sunitinib in personalized chemotherapy. (*Cancer Sci* 2010; 101: 1493–1500)

The ATP-binding cassette (ABC) transporter proteins, particularly P-glycoprotein (P-gp/ABCB1), multidrug resistance-associated protein 1 (MRP1/ABCC1), and breast cancer resistance protein (BCRP/MXR/ABCP/ABCG2) have been extensively studied as key molecules that are involved in the multidrug-resistant phenotype of cancer cells.[1,2] P-gp effluxes various anticancer agents including vincristine (VCR), paclitaxel (PTX), doxorubicin (DOX), and mitoxantrone (MXR).[1,3] BCRP is referred to as a half-type ABC transporter that functions as a homodimer and transports anticancer agents such as topotecan, irinotecan, SN-38 (7-ethyl-10-hydroxycamptothecin), methotrexate, and MXR out of cells.[4]

Many compounds have been tested for their ability to overcome ABC transporter-mediated drug resistance. Verapamil, cyclosporine A (CsA), and other compounds have been identified as inhibitors of P-gp,[5,6] while fumitremorgin C (FTC), tamoxifen derivatives, and certain flavonoids inhibit BCRP.[7–10] Verapamil, for example, directly interacts with P-gp and competitively interferes with transporter–substrate binding.[11] Co-administration of inhibitory compounds would be expected to overcome unwanted anticancer drug resistance during chemotherapy, but is also suspected to affect the pharmacokinetics and pharmacodynamics of substrate anticancer drugs.

Recent genetic analyses of the multidrug resistance gene 1 (*MDR1*) and *BCRP* genes have revealed that some germ-line mutations, including single nucleotide polymorphisms (SNP), affect the pharmacological activities of these ABC transporters.[3,12,13] We previously reported that the germ-line mutant allele 3587T>G in *MDR1* expresses a nonfunctional P-gp.[14] We also reported variant *BCRP* SNP cDNAs harboring 421C>A (amino acid substitution Q141K),[15] and this SNP is physiologically important because the pharmacokinetics of diflomotecan, a new camptothecin-derivative anticancer agent, and the risk of adverse reactions, such as gefitinib-induced diarrhea, was affected in patients heterozygous for the A421 allele.[16] In addition, we reported that a germ-line mutant allele 1291T>C expresses the F431L variant of BCRP with lower functional resistance to SN-38.[17] This suggests that amino acid substitution F431L may affect substrate recognition of SN-38.

The small-molecule TKIs, most of which are competitive inhibitors for ATP, are currently used in various clinical settings.[18] Sunitinib malate (Sutent) is an unique ATP-competitive multitargeted TKI that inhibits platelet-derived growth factor receptor (PDGFR) α and β, vascular endothelial cell growth factor receptor (VEGFR) types 1 and 2, stem cell factor receptor c-KIT, FMS-like TK-3 receptor, and the glial cell-line-derived neutrophic factor receptor.[19] Sunitinib was approved by the Food and Drug Administration in the USA in 2006 and in Japan in 2008 for the treatment of advanced renal cell carcinoma and imatinib-resistant gastrointestinal stromal tumor.

Recent studies have shown pharmacological interaction between several clinically important TKIs with the ABC transporters P-gp and BCRP.[20–27] Regarding pharmacological properties, imatinib, gefitinib, erlotinib, and sunitinib can inhibit the function of ABC transporters and might cause unexpected adverse effects during novel combination chemotherapy with these TKIs and other drugs in early clinical trials.[28–31] Unfortunately, as in our recent report, the pharmacological inhibitory effects of TKIs on ABC transporters are dependent upon the pairings between the transporter protein, the substrate drug, and TKIs.[32] Moreover, genetic polymorphisms of the ABC transporters are associated with modulations in functional transporter activity.[4,33] Therefore, it is difficult to predict the possible pharmacological interactions between TKIs, anticancer drugs, and ABC transporters in individual patient based on the current insufficient evidence.

Sunitinib is expected to be examined for use in combination with conventional chemotherapies in various tumor settings. Most recently, sunitinib was shown to antagonize P-gp- and BCRP-mediated drug resistance through direct inhibition of their efflux activities.[26,27] In the present study, we found

[1]To whom correspondence should be addressed.
E-mail: sugimoto-ys@pha.keio.ac.jp

doi: 10.1111/j.1349-7006.2010.01539.x

that the inhibitory effects of sunitinib on P-gp and BCRP are mediated by a competitive mechanism. Moreover, we show for the first time that this inhibitory effect of sunitinib on BCRP is cancelled by a germ-line mutation of *BCRP* gene (1291T>C) that causes a single amino acid substitution of F431L.

Materials and Methods

Reagents. Sunitinib was kindly provided by Pfizer (Groton, CT, USA). SN-38 was provided by Yakult Honsha (Tokyo, Japan). Other chemicals were commercially available. The anti-BCRP polyclonal antibody 3488 was generated as described elsewhere.[34]

Cells and drug sensitivity assay. PA317 mouse fibroblast cells, K562 human myelogenous leukemia cells, BCRP-expressing PA317 cells, BCRP-expressing K562 cells (K562/BCRP), and P-gp-expressing K562 cells (K562/MDR) were established and cultured as previously.[17,21] To establish K562/F431L cells, parental K562 cells were transduced with a HaBCRP retrovirus-harboring Myc-tagged human *BCRP* (F431L) cDNA in the Ha retrovirus vector as previously described.[17] After limiting dilution without any selective drugs and screening of over 700 clones, we selected two F431L-BCRP-expressing K562 cell clones K562/F431L-1 and -3.

To enrich BCRP-expressing PA317 cells, cells were labeled with biotin-labeled anti-BCRP antibody, and antibody-attached BCRP-expressing cells were purified by a magnetic beads system using a MACS streptavidin kit (Miltenyi Biotec, Bergisch Gladbach, Germany). This purification procedure was repeated three or four times, and the cell surface expression of BCRP was confirmed by fluorescence analysis.

The chemosensitivity of the PA317 and K562 cell lines in the presence or absence of sunitinib was evaluated by a cell growth assay in which cell numbers were counted using a Coulter counter or by MTT assay after incubation of the cells for 5 days. The IC_{50} values (dose of drug achieving 50% inhibition) and the reversal indices (RI_{50}) (concentration of inhibitors sunitinib, CsA, or FTC) that caused a twofold reduction in the IC_{50} values for anticancer drugs in each resistant cell line) were defined as previously described.[10]

Intravesicular transport assay. The vesicular transport assay was done using a rapid centrifugation technique with ^{3}H-labeled VCR and estrone 3-sufate (E_1S) (Perkin-Elmer Life Sciences, Boston, MA, USA), essentially as described before.[21,32] For Lineweaver–Burk plot analysis, the concentrations of ^{3}H-labeled VCR were 100, 200, and 400 nmol/L for K562/MDR vesicles, and concentrations of E_1S were 50, 100, and 200 nmol/L for K562/BCRP vesicles.

Intracellular accumulation of mitoxantrone and VCR. The effect of sunitinib on cellular accumulation of MXR was determined by flow cytometry as described before.[32] In brief, 5×10^5 K562, K562/BCRP or K562/MDR cells were incubated with 1 μmol/L of MXR for 40 min at 37°C in the absence or presence of sunitinib (1, 3, and 10 μmol/L), CsA (1, 3, and 10 μmol/L), or FTC (1, 3, and 10 μmol/L). MXR fluorescence was measured using a BD LSR II system (Becton Dickinson, San Jose, CA, USA). The cellular uptake of VCR was determined by intracellular accumulation of ^{3}H-labeled VCR (American Radiolabelled Chemicals, St. Louis, MO, USA). In brief, cells were pre-incubated with 10 μmol/L sunitinib or CsA for 5 min, and then cultured in the presence of 100 nmol/L of ^{3}H-labeled VCR for 20 min and washed three times with ice-cold PBS. The cell pellets were then solubilized and radioactivity was measured using a liquid scintillation counter.

Cellular efflux assay. Cellular efflux assay was done as described before.[32] In brief, cells were incubated with 0.2 μmol/L of ^{3}H-labeled MXR or VCR for 30 min at 37°C, and washed twice with ice-cold PBS, and suspended in ice-cold ^{3}H-free fresh normal growth medium. At the indicated times, supernatants were collected to measure efflux of [^{3}H] radioactivity levels using a liquid scintillation counter.[32]

Cell surface BCRP expression. The cell surface expression of BCRP was determined by fluorescence analysis. Cells were incubated with or without a biotinylated human-specific monoclonal antibody raised against BCRP (5D3) (100 μg/mL). The cells were then washed and incubated with R-phycoerythrin-conjugated streptavidin (400 μg/mL; Becton Dickinson) and fluorescence levels were detected using a BD LSR II system (Becton Dickinson).

Western blot analysis and photoaffinity labeling with iodoarylazidoprazosin (IAAP). Western blotting was performed as previously reported.[17] The photoaffinity labeling assay was done, essentially as previously described.[26] In brief, membrane vesicle fractions from BCRP-expressing K562 cells (90 μg protein/sample) were pre-incubated with 0 or 10 μmol/L sunitinib or FTC for 5 min at room temperature in 50 mmol/L Tris-HCl (pH 7.5). Then, 10 nmol/L [^{125}I]IAAP (2200 Ci/mmol) (Perkin-Elmer Life Sciences) was added and incubated for an additional 10 min. The sample plate was kept on ice and illuminated with a UV lamp (365 nm, UVP LLC, model B-100AP; Upland, CA, USA) for 30 min at room temperature. The labeled BCRP protein was solubilized in a buffer containing 1% NP-40, 0.1% sodium deoxycholate, 20 mmol/L Tris-HCl (pH 7.5), 150 mmol/L NaCl, 1 mmol/L EDTA, and immunoprecipitated with the anti-BCRP antibody BXP-21 (Millipore, Billerica, MA, USA). Samples were separated by 5–20% SDS–PAGE, and the gels were dried. The binding of [^{125}I]IAAP with BCRP was quantified using the FLA7000 Bio-image analyzer (Fujifilm, Tokyo, Japan) with the software Multi-Gauge (Fujifilm).

Results

Suppressive effects of sunitinib on BCRP- and P-gp-mediated drug resistance. The sunitinib dose-dependently overcame the relative resistance to SN-38 and MXR in K562/BCRP cells (Fig. 1a and Fig. S1a, Supporting information). The RI_{50} value for sunitinib, the concentration that caused a 2-fold reduction in the IC_{50} for SN-38 and MXR in K562/BCRP cells, was calculated as shown in Table 1. The RI_{50} values of sunitinib for SN-38 and MXR were comparable with those of FTC (0.09 and 0.19 mmol/L) and erlotinib (0.05 and 0.1 mmol/L) as shown in our recent report.[32] Collectively, sunitinib and FTC appeared to exhibit equivalent inhibitory activities against BCRP-mediated drug resistance in K562/BCRP cells.

We next tested the effects of sunitinib on P-gp-mediated drug resistance in K562/MDR cells. K562/MDR cells were resistant to VCR (relative resistance: ~390-fold), PTX (~450-fold), DOX (~20-fold), and MXR (~6-fold), and the effects of sunitinib on overcoming the resistance of K562/MDR cells to these drugs were weak (Fig. 1b). The dose-dependent effect of sunitinib on P-gp-mediated drug resistance was analyzed (Fig. 1b) and the RI_{50} value of sunitinib on K562/MDR cells was determined as shown in Table 2. These experiments indicated that P-gp-mediated resistance to DOX and MXR was not inhibited by sunitinib although sunitinib partially reversed P-gp-mediated resistance to VCR and PTX, with RI_{50} values for sunitinib of 0.44 and 0.3 mmol/L, respectively. As a typical inhibitor for P-gp, CsA was subjected to the same experiments (Fig. S1c, Supporting information), and the results showed that CsA reversed P-gp-mediated drug resistance to VCR, PTX, DOX, and MXR in K562/MDR cells equivalently (Table 2 and Fig. S1c, Supporting information).

Sunitinib co-treatment consistently increased the intracellular accumulation of MXR and suppressed MXR efflux through BCRP with an efficacy that was similar to FTC (Fig. 2a–c).

doi: 10.1111/j.1349-7006.2010.01539.x

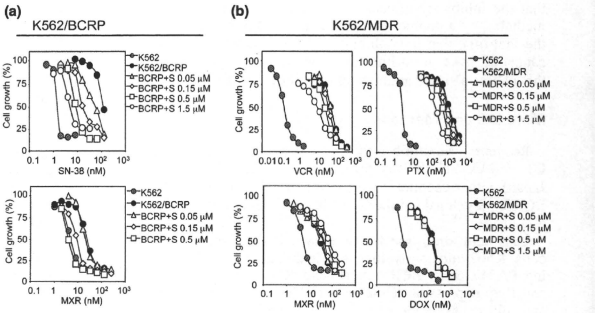

Fig. 1. Overcoming drug resistance using sunitinib. The chemosensitivity of K562/breast cancer resistance protein (BCRP) (a) and K562/multidrug resistance protein (MDR) cells (b) to anticancer drugs were determined without (filled circles) or with sunitinib (0.05 μmol/L, open triangles; 0.15 μmol/L, open diamonds; 0.5 μmol/L, open squares; 1.5 μmol/L, open circles). Chemosensitivity of parental K562 cells is shown in gray circles. Cell growth inhibition after 5 days of culture was determined using the MTT assay. The growth inhibition curves were established from the means ± SD from triplicate determinations.

Table 1. Reversal of BCRP-mediated drug resistances

	RI_{50} values (μmol/L) for K562/BCRP
	Sunitinib
MXR	0.10 ± 0.003
SN-38	0.064 ± 0.004

Results are means ± SD of triplicate experiments. BCRP, breast cancer resistance protein; MXR, mitoxantrone; RI_{50}, 50% reversal index; SN-38, 7-ethyl-10-hydroxycamptotecin.

Table 2. Reversal of P-gp-mediated drug resistances

	RI_{50} values (μmol/L) for K562/MDR	
	Sunitinib	CsA
VCR	0.44 ± 0.02	0.17 ± 0.004
PTX	0.30 ± 0.06	0.20 ± 0.02
DOX	Not determined	0.29 ± 0.02
MXR	Not determined	0.24 ± 0.01

Results are means ± SD of triplicate experiments. CsA, cyclosporin A; DOX, doxorubicin; MXR, mitoxantrone; PTX, paclitaxel; RI_{50}, 50% reversal index; VCR, vincristine.

In contrast, sunitinib did not in K562/MDR cells (Fig. 2d–f). However, sunitinib partially suppressed P-gp-mediated VCR efflux and increased intracellular VCR accumulation in K562/MDR cells (Fig. 2g,h). Therefore, the inhibitory effect of sunitinib on P-gp appeared to be different from that of CsA, and our observations indicate that the inhibitory effects of sunitinib were dependent on the specific substrate involved in the P-gp-mediated resistance phenotype.

Effects of sunitinib on BCRP- and P-gp-mediated transports. An intravesicular transport assay was performed to analyze the kinetics of sunitinib inhibition on BCRP-mediated transport *in vitro* using membrane vesicles from K562/BCRP cells. As shown in Figure 3(a), ATP-dependent [^{3}H]E_1S transport was dose-dependently inhibited by sunitinib, similar to that with FTC (IC_{50} values for sunitinib and FTC: 0.24 and 0.28 μmol/L, respectively). Moreover, the Lineweaver–Burk plot analysis showed that sunitinib acted as a competitive inhibitor for BCRP-mediated E_1S transport (Fig. 3b). The calculated *Vmax* (pmol/mg/min) was 8.8 for the control condition, 6.1 for sunitinib (at 1 μmol/L), and 8.5 for FTC (at 1 μmol/L), and the calculated *Ki* values for sunitinib and FTC were both 0.32 μmol/L. Therefore, sunitinib acts as a competitive inhibitor for BCRP-mediated E_1S transport, and our analysis revealed that sunitinib and FTC have equivalent inhibitory activity on BCRP.

Although sunitinib did not inhibit P-gp-mediated MXR efflux (as shown in Figs 1,2 and Fig. S1, Supporting information), sunitinib partially overcame P-gp-mediated VCR resistance in K562/MDR cells (Figs 1b,2g,h and Fig. S1b, Supporting information). Therefore, we examined the effect of sunitinib on P-gp-mediated VCR transport by a transport assay using membrane vesicles from K562/MDR cells and [^{3}H]VCR as a transporter substrate. These experiments showed that both sunitinib and CsA inhibited P-gp-mediated VCR transport (Fig. 3c). However, while 10 mmol/L CsA completely suppressed VCR transport, a higher concentration (30 mmol/L) of sunitinib was required for complete inhibition of P-gp-mediated VCR transport, indicating that the inhibitory activity of sunitinib was weaker than that of CsA, with IC_{50} values of 16.2 and 2.2 μmol/L, respectively. The Lineweaver–Burk plot analysis (Fig. 3d) indicated that the calculated *Vmax* values for control, sunitinib (at 15 μmol/L)-treated and CsA (at 5 μmol/L)-treated samples were similar (21.3, 17.5, and 16.7 pmol/mg/min, respectively). The calculated *Ki* value for sunitinib was about 7.6 μmol/L and that for CsA was about 1.3 μmol/L for P-gp-mediated VCR transport. Therefore, the inhibitory mode of sunitinib for P-gp-mediated VCR transport appeared to involve competition, similar to that of CsA. Our analysis also suggested that the inhibitory activity of sunitinib for P-gp is weaker than that of CsA. Overall, these results indicate that sunitinib acts as a competitive inhibitor on the transporter function of BCRP and P-gp, and that sunitinib shows better activity against BCRP than against P-gp.

Effects of sunitinib on BCRP variants. Previous molecular cloning studies of *BCRP* cDNAs from drug-selected cells and normal tissues have uncovered functional variants of BCRP with amino acid substitutions and their substrate preferences.[13,35–37] The Q141K variant, a widespread SNP in Japanese individuals, is associated with the low protein expression of BCRP,[15] and the F431L variant, also a germ-line mutation of BCRP, shows a low level of resistance to SN-38. The R482T and R482G are BCRP variants identified after *in vitro* selection of culture cells and these variants confer DOX- and MXR-resistances.[34] Before examining the suppressive effect of sunitinib on these BCRP variant-expressing murine fibroblast PA317 cells, cell populations with high BCRP expression were selectively enriched using immunomagnetic beads. The BCRP protein expression levels were confirmed to be comparable between each enriched variant BCRP-expressing PA317 cells (Fig. S2a–c, Supporting information). Using these cells, we determined the drug resistance of BCRP-expressing cells to SN-38 with or without various concentrations of sunitinib (Fig. 4a), and sunitinib-mediated reversal of the relative resistance to SN-38 was calculated (Fig. 4b). To our surprise, sunitinib showed only

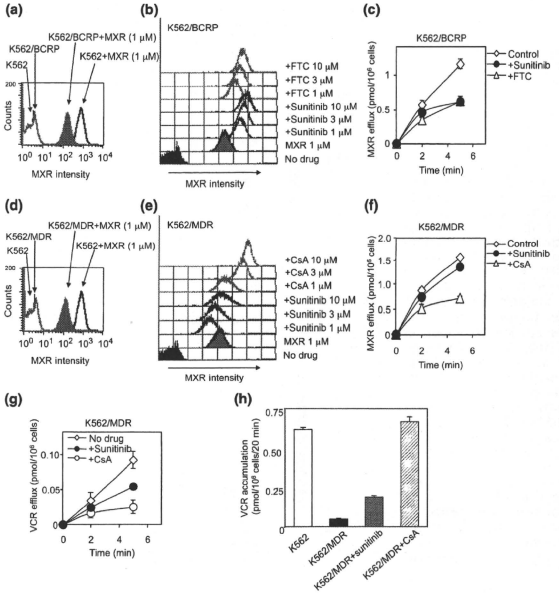

Fig. 2. Effects of sunitinib on the uptake and efflux of mitoxantrone (MXR). Intracellular accumulation of MXR in K562 as a control, K562/breast cancer resistance protein (BCRP) (a) and K562/multidrug resistance protein (MDR) (d) cells was determined as the fluorescence intensity of MXR measured by flow cytometry. The histogram for MXR fluorescence intensity shows the intracellular accumulation level of MXR. The cellular uptake of MXR in the presence of sunitinib or fumitremorgin C (FTC) (b, gray lines) or cyclosporine A (CsA) (e, gray lines) in K562/BCRP (b, bold lines), and K562/MDR (e, bold lines) cells was measured as above. The fluorescence intensity patterns without MXR (control) are shown as filled histograms, and those without inhibitors as gray histograms. To measure the cellular efflux of MXR, K562/BCRP (c) and K562/MDR (f) cells were pre-treated with 200 nmol/L of ^{3}H-labeled MXR for 30 min and then incubated in fresh growth medium without ^{3}H-labeled MXR. The efflux of ^{3}H-labeled MXR was determined by measuring the level of radioactivity exported into the culture medium. The time-dependent efflux of MXR in the absence of inhibitors is shown as open diamond symbols (c,f). The effects of sunitinib (filled circles), FTC (c, open triangles), and cyclosporine A (CsA) (f, open triangles) on MXR efflux were determined. Results are means ± SD of triplicate determinations. (g) To measure cellular efflux of VCR, K562/MDR cells were pre-treated with 100 nmol/L of ^{3}H-labeled VCR for 30 min and then incubated in fresh growth medium without ^{3}H-labeled VCR. The efflux of ^{3}H-labeled VCR was determined as above. The time-dependent efflux of VCR in the presence of sunitinib (filled circles), CsA (open circles) or absence of inhibitor (open diamond symbols) is shown. (h) Cellular uptake of VCR in K562/MDR cells was determined in the absence or presence of 10 μmol/L of inhibitors. The accumulation of VCR is shown for parental K562 (white column), K562/MDR (black column), K562/MDR cells with sunitinib (gray column), and K562/MDR cells with CsA (hatched column). Results are means ± SD of triplicate determinations.

marginal ability to overcome SN-38 resistance in the F431L-BCRP variant, even though the other BCRP variants were all sensitive to sunitinib with comparable efficacy.

To confirm these observations, we also tested the effect of sunitinib on F431L-BCRP in different cell lines. The F431L BCRP-expressing K562 cell clones K562/F431L-1 and -3 were established without the drug selection process. FACS analysis showed that the protein expression of F431L-BCRP in K562 cells was relatively low (1/8–1/4-fold compared with wild-type BCRP-expressing K562 cells) (Fig. 5a). The reason for the lower protein expression of F431L-BCRP in K562 cells is unknown, but we could not isolate K562/F431L clones expressing high levels of F431L-BCRP protein, even after the screening of over 700 clones. These additional experiments also revealed that sunitinib could not overcome SN-38 resistance conferred by F431L-BCRP (Fig. 5b). We also examined the inhibition of the F431L-BCRP variant by the typical BCRP inhibitor FTC and found that the F431L-BCRP variant was also resistant to FTC-mediated inhibition (Fig. 5c). These data suggested that the residue Phe-431 of BCRP would be important for the interaction with sunitinib and FTC.

Effects of sunitinib on IAAP binding to F431L-BCRP. We next examined the effect of sunitinib on photoaffinity labeling of wild-type and F431L-BCRP with [I^{125}]IAAP-binding to investigate the direct competition between the substrate IAAP and sunitinib on the F431L variant. Because F431L-BCRP protein expression was lower than wild-type BCRP in K562 cell lines (Fig. 6a), [I^{125}]IAAP-binding to the membrane vesicles prepared from these K562/F431L cells was weaker than that from wild-type BCRP-expressing membrane vesicles. Consistent with other reports, sunitinib (10 μmol/L) and FTC (10 μmol/L) inhibited [I^{125}]IAAP-binding to wild-type BCRP, whereas [I^{125}]IAAP-binding to the F431L variant was apparently resistant to sunitinib- and FTC-mediated inhibition (Fig. 6b,c). These data clearly showed that the F431L variant has decreased affinity for physical interactions with sunitinib and FTC.

doi: 10.1111/j.1349-7006.2010.01539.x

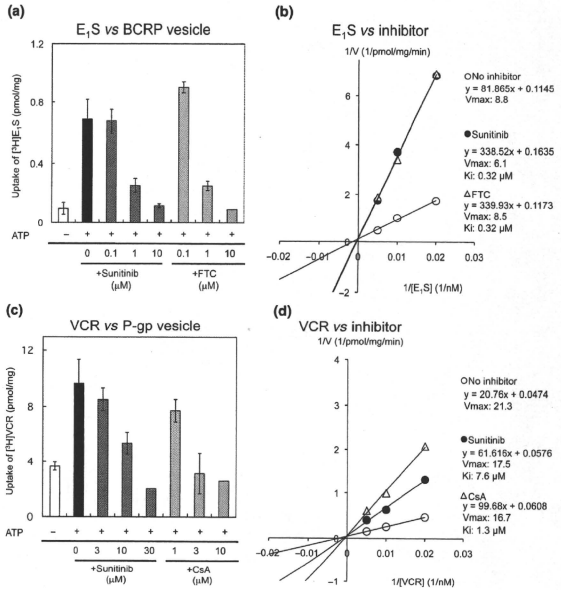

Fig. 3. The intravesicular transport of estrone 3-sufate (E_1S) by breast cancer resistance protein (BCRP) and of vincristine (VCR) by P-glycoprotein (P-gp). (a) The transport of [^{3}H]E_1S was determined by measuring the radioactivity incorporated into the membrane vesicles from K562/BCRP cells, as described in the Materials and Methods. (b) Lineweaver–Burk plot analysis was used to determine the mode of sunitinib inhibition of BCRP in the intravesicular transport assay. The concentration of ^{3}H-labeled E_1S was 50 nmol/L in experiments (a) and 50, 100, and 200 nmol/L, respectively in (b). Sunitinib at 1 μmol/L and FTC at 1 μmol/L were tested in experiment (b). (c) Effects of sunitinib on VCR transport by P-gp. The transport of [^{3}H]VCR was determined using membrane vesicles from K562/MDR cells as above. (d) Lineweaver–Burk plot analysis was performed to determine the mode of sunitinib inhibition of P-gp. The concentration of ^{3}H-labeled VCR was 100 nmol/L in the experiments (c) and 100, 200, and 400 nmol/L, respectively, in (d). Sunitinib at 15 μmol/L and CsA at 5 μmol/L were tested in experiment (d). Results shown in (a) and (c) are means ± SD of triplicate determinations, and results in (b) and (d) are means of duplicate determinations.

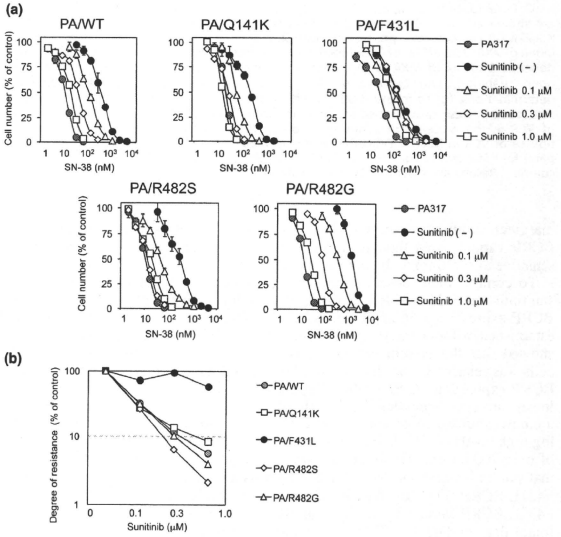

Fig. 4. Sunitinib overcomes variant breast cancer resistance protein (BCRP)-mediated drug resistance. (a) Variant BCRP-expressing PA317 cell lines were cultured for 5 days with SN-38 and sunitinib. Cell numbers were determined with a Coulter counter and the cell growth inhibition curves (% of control) are shown. Results are means ± SD of triplicate determinations. (b) BCRP-mediated resistance to SN-38 in the presence of sunitinib was determined as IC_{50} values and relative resistance was calculated as the ratio of the IC_{50} value in the presence of sunitinib divided by the IC_{50} value in the absence of sunitinib. Reversal ratios are shown for wild-type (gray circles), and Q141K (open squares), F431L (filled circles), R482S (open diamonds), and R482G (open triangles) BCRP variant-expressing cells.

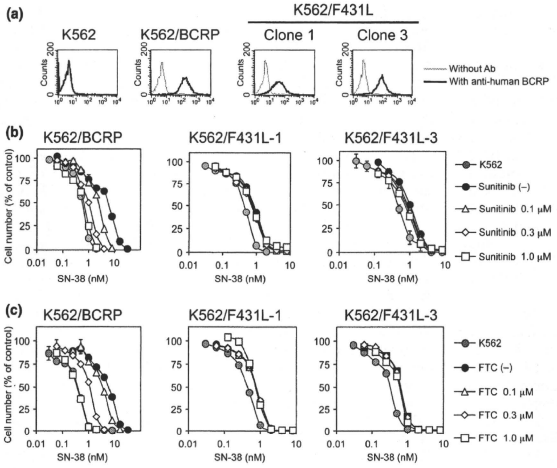

Fig. 5. Sunitinib failed to overcome F431L-breast cancer resistance protein (BCRP)-mediated drug resistance in K562 cells. Protein expression of BCRP in K562/F431L cells was analyzed by flow cytometry (a). The F431L-BCRP-expressing K562 cell lines K562/F431L-1 and -3 were cultured for 5 days with SN-38 and sunitinib (b) or fumitremorgin C (FTC) (c). Cell growth was determined with a Coulter counter and cell growth inhibition curves (% of control) are shown. Results are means ± SD of triplicate determinations.

Overall, our results indicate that sunitinib can inhibit the transporter function of both BCRP and P-gp, albeit less efficiently for P-gp. Moreover, the germ-line BCRP variant F431L showed decreased affinity for sunitinib and therefore would be irrelevant to the pharmacological and physical interaction between BCRP and sunitinib.

Discussion

Various small-molecule TKIs can modulate the functional activity of ABC transporters such as P-gp, BCRP, and MRP1.[38–40] We have studied the mode of action of TKIs and ABC transporters, and previously reported the effects of gefitinib and erlotinib on BCRP and P-gp. We showed that gefitinib and erlotinib are competitive inhibitors for BCRP, while erlotinib is a complex-type inhibitor for P-gp.[21,32,41] In this study, we first examined the activity of sunitinib as a competitive inhibitor for both BCRP and P-gp, and found that BCRP appeared to be a better target for sunitinib than P-gp. Second, we investigated the effect of sunitinib on mutants of BCRP, and found that the F431L variant conferred resistance to sunitinib-mediated suppression. Thus, this is the first report showing that the germ-line mutation of *BCRP/ABCG2* affects the pharmacological interaction with TKIs.

A study by Shukla *et al.* demonstrated that inhibitory effect of sunitinib on P-gp-mediated drug resistance appeared to be partial compared with that on BCRP, and that the ATPase activity of P-gp was stimulated by higher concentrations of sunitinib than were required for BCRP.[26] Dai *et al.* reported no significant effect of sunitinib on P-gp-mediated drug resistance.[27] In our experiments, sunitinib partially suppressed P-gp-mediated resistance to VCR and PTX at sub-micromolar concentrations, but did not to DOX and MXR. The P-gp drug interaction sites are thought to be localized to the transmembrane domains and the presence of multiple drug-binding sites has been suggested.[42] The physical interaction sites for MXR and DOX are not well defined for P-gp, and the interaction mode of *vinca* alkaloids with P-gp seems to be different from that of DOX.[42] Our data suggest that the putative region on P-gp that interacts with sunitinib may be associated with the VCR-binding site, but

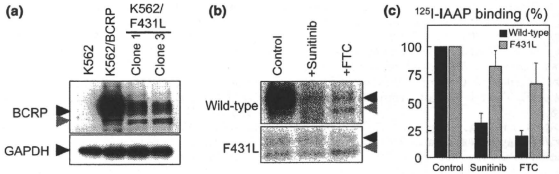

Fig. 6. Effect of sunitinib on photoaffinity labeling of wild-type and F431L-breast cancer resistance protein (BCRP) with [^{125}I]IAAP. Protein expression of BCRP was analyzed by western blotting (a) in F431L-*BCRP*-transduced K562 cells. Membrane vesicles (90 μg/mL) from K562/BCRP and K562/F431L-3 cells were pre-incubated for 5 min with sunitinib or fumitremorgin C (FTC) (10 μmol/L each) and then 10 nmol/L of [^{125}I]IAAP was added for a further 10 min. After cross-linking by UV irradiation, BCRP proteins were immunoprecipitated and resolved by SDS–PAGE. The binding of [^{125}I]IAAP to BCRPs was visualized (b) and quantified (c) with an FLA7000 instrument. Black and gray arrowheads are BCRP protein as described in reference 17. A representative result of three independent experiments is shown in (b) and the means and SD from three independent experiments are shown in (c).

doi: 10.1111/j.1349-7006.2010.01539.x

is distinct from the DOX interaction site. Further molecular studies are required to elucidate the modes of interaction between sunitinib and P-gp.

The germ-line mutant F431L-BCRP was previously shown to have low ability to confer drug-resistance to SN-38.[34] Our present study also showed that the F431L mutation in BCRP compromised the pharmacological and physical interactions with sunitinib and FTC. Regarding the physical interaction between TKIs and BCRP, gefitinib binds to ATP-bound BCRP at an as yet unknown binding site,[43] while erlotinib stimulates the ATPase activity of BCRP but does not compete with IAAP-binding to BCRP.[23] By contrast, a study by Shukla *et al.* and our data showed a direct interaction between sunitinib and IAAP-binding sites on BCRP and P-gp.[26] Thus F431L substitution may reduce substrate/inhibitor-recognition efficacy or may be an important amino acid residue involved in the functional transporter activity of BCRP.

Phe-431 is thought to be located near the boundary region between the extracellular side and the second transmembrane domain of BCRP,[44,45] but it is still unclear whether Phe-431 is associated with the substrate-binding pocket. Li *et al.* reported that another mutant, F431S-BCRP, is still functional because pheophorbide A transport by F431S-BCRP was completely suppressed by FTC.[44] Therefore, they excluded the possible importance of the Phe-431 residue at the BCRP dimer interface and proposed that Phe-431 faced the lipid bilayer. Our observations also indicate that the F431L-BCRP protein forms a dimer (data not shown), but our data appeared to be inconsistent with their conclusion because the F431L-BCRP variant showed reduced sensitivity to FTC. Unfortunately, we failed to confirm the inhibitory effects of sunitinib and FTC on F431L-BCRP-mediated drug transport using the *in vitro* vesicle transport assay because the membrane vesicles prepared from K562/F431L cells did not show good transport activity *in vitro* (data not shown). However, we also monitored anti-BCRP antibody 5D3 reactivity to F431L-BCRP in the presence or absence of FTC because the direct interaction between FTC and BCRP is thought to stimulate the binding efficacy of the anti-BCRP antibody 5D3 by inducing a conformational change in BCRP.[46] In this 5D3 reactivity test, the fluorescence intensity associated with 5D3 antibody binding was changed by FTC treatment in K562/BCRP cells, but not in K562/F431L cells (Fig. S3, Supporting information). This experiment suggested that F431L-BCRP is resistant to the FTC-induced conformational change required for 5D3 antibody-binding to BCRP. Overall, we suspect that the F431L variant shows compromised physical interaction with FTC and sunitinib, or altered conformational dynamics that are required for substrate recognition and transport cycling by BCRP.

It is likely that sunitinib administration not only modulates the normal functions of BCRP expressed in digestive organs, the kidney, and the blood–brain barrier, but is also likely to influence the efficacy of anticancer drugs during combination chemotherapy.[31] Although F431L-BCRP had lower transporter activity than wild-type BCRP, this mutant BCRP still conferred significant drug-resistance in both PA317 and K562 cells, so that we should pay attention to functional relevance between drug–drug interaction and this mutant BCRP. Importantly, our findings demonstrate that germ-line mutations of the *BCRP/ABCG2* gene 1291T>C (F431L), affect its pharmacological interaction with sunitinib. Recent pharmacogenetic analyses revealed that two polymorphisms (−15622C/T and 1143C/T) of the *BCRP/ABCG2* gene that result in reduced BCRP expression are strongly associated with erlotinib- and sunitinib-induced cytotoxicity in patients.[30,31] Taken together, the results of studies investigating the pharmacological interaction between TKIs, ABC transporters, and their substrates should contribute to the understanding of the molecular basis of the pharmacokinetics of sunitinib and other drugs used in chemotherapy. In future personalized medicine, functional analysis of germ-line mutation affecting efficacy of drug–drug interactions such as F431L-BCRP with sunitinib would contribute to design for the evidence-based optimized chemotherapy regimen in each patient.

Acknowledgments

This work was supported by Grants-in-Aid from the Ministry of Education, Culture, Sports, Science and Technology, and from the Ministry of Health, Labor and Welfare of Japan. We thank Yuka Shimomura for performing the initial experiments in this study, and other laboratory members for their helpful discussions.

References

1 Gottesman MM, Fojo T, Bates SE. Multidrug resistance in cancer: role of ATP-dependent transporters. *Nat Rev Cancer* 2002; **2**: 48–58.
2 Leslie EM, Deeley RG, Cole SP. Multidrug resistance proteins: role of P-glycoprotein, MRP1, MRP2, and BCRP (ABCG2) in tissue defense. *Toxicol Appl Pharmacol* 2005; **204**: 216–37.
3 Ambudkar SV, Kimchi-Sarfaty C, Sauna ZE, Gottesman MM. P-glycoprotein: from genomics to mechanism. *Oncogene* 2003; **22**: 7468–85.
4 Sugimoto Y, Tsukahara S, Ishikawa E, Mitsuhashi J. Breast cancer resistance protein: molecular target for anticancer drug resistance and pharmacokinetics/pharmacodynamics. *Cancer Sci* 2005; **96**: 457–65.
5 Tsuruo T, Iida H, Tsukagoshi S, Sakurai Y. Overcoming of vincristine resistance in P388 leukemia *in vivo* and *in vitro* through enhanced cytotoxicity of vincristine and vinblastine by verapamil. *Cancer Res* 1981; **41**: 1967–72.
6 Leonard GD, Fojo T, Bates SE. The role of ABC transporters in clinical practice. *Oncologist* 2003; **8**: 411–24.
7 Rabindran SK, Ross DD, Doyle LA, Yang W, Greenberger LM. Fumitremorgin C reverses multidrug resistance in cells transfected with the breast cancer resistance protein. *Cancer Res* 2000; **60**: 47–50.
8 Sugimoto Y, Tsukahara S, Imai Y, Ueda K, Tsuruo T. Reversal of breast cancer resistance protein-mediated drug resistance by estrogen antagonists and agonists. *Mol Cancer Ther* 2003; **2**: 105–12.
9 Imai Y, Tsukahara S, Asada S, Sugimoto Y. Phytoestrogens/flavonoids reverse breast cancer resistance protein/ABCG2-mediated multidrug resistance. *Cancer Res* 2004; **64**: 4346–52.
10 Katayama K, Masuyama K, Yoshioka S, Hasegawa H, Mitsuhashi J, Sugimoto Y. Flavonoids inhibit breast cancer resistance protein-mediated drug resistance: transporter specificity and structure-activity relationship. *Cancer Chemother Pharmacol* 2007; **60**: 789–97.
11 Yusa K, Tsuruo T. Reversal mechanism of multidrug resistance by verapamil: direct binding of verapamil to P-glycoprotein on specific sites and transport of verapamil outward across the plasma membrane of K562/ADM cells. *Cancer Res* 1989; **49**: 5002–6.
12 Iida A, Saito S, Sekine A *et al.* Catalog of 605 single-nucleotide polymorphisms (SNPs) among 13 genes encoding human ATP-binding cassette transporters: ABCA4, ABCA7, ABCA8, ABCD1, ABCD3, ABCD4, ABCE1, ABCF1, ABCG1, ABCG2, ABCG4, ABCG5, and ABCG8. *J Hum Genet* 2002; **47**: 285–310.
13 Yanase K, Tsukahara S, Mitsuhashi J, Sugimoto Y. Functional SNPs of the breast cancer resistance protein-therapeutic effects and inhibitor development. *Cancer Lett* 2006; **234**: 73–80.
14 Mutoh K, Mitsuhashi J, Kimura Y *et al.* A T3587G germ-line mutation of the MDR1 gene encodes a nonfunctional P-glycoprotein. *Mol Cancer Ther* 2006; **5**: 877–84.
15 Imai Y, Nakane M, Kage K *et al.* C421A polymorphism in the human breast cancer resistance protein gene is associated with low expression of Q141K protein and low-level drug resistance. *Mol Cancer Ther* 2002; **1**: 611–6.
16 Sparreboom A, Gelderblom H, Marsh S *et al.* Diflomotecan pharmacokinetics in relation to ABCG2 421C>A genotype. *Clin Pharmacol Ther* 2004; **76**: 38–44.
17 Yoshioka S, Katayama K, Okawa C *et al.* The identification of two germ-line mutations in the human breast cancer resistance protein gene that result in the expression of a low/non-functional protein. *Pharm Res* 2007; **24**: 1108–17.
18 Steeghs N, Nortier JW, Gelderblom H. Small molecule tyrosine kinase inhibitors in the treatment of solid tumors: an update of recent developments. *Ann Surg Oncol* 2007; **14**: 942–53.

19 Chow LQ, Eckhardt SG. Sunitinib: from rational design to clinical efficacy. *J Clin Oncol* 2007; **25**: 884–96.
20 Burger H, van Tol H, Boersma AW *et al.* Imatinib mesylate (STI571) is a substrate for the breast cancer resistance protein (BCRP)/ABCG2 drug pump. *Blood* 2004; **104**: 2940–2.
21 Yanase K, Tsukahara S, Asada S, Ishikawa E, Imai Y, Sugimoto Y. Gefitinib reverses breast cancer resistance protein-mediated drug resistance. *Mol Cancer Ther* 2004; **3**: 1119–25.
22 Elkind NB, Szentpetery Z, Apati A *et al.* Multidrug transporter ABCG2 prevents tumor cell death induced by the epidermal growth factor receptor inhibitor Iressa (ZD1839, Gefitinib). *Cancer Res* 2005; **65**: 1770–7.
23 Shi Z, Peng XX, Kim IW *et al.* Erlotinib (Tarceva, OSI-774) antagonizes ATP-binding cassette subfamily B member 1 and ATP-binding cassette subfamily G member 2-mediated drug resistance. *Cancer Res* 2007; **67**: 11012–20.
24 Brendel C, Scharenberg C, Dohse M *et al.* Imatinib mesylate and nilotinib (AMN107) exhibit high-affinity interaction with ABCG2 on primitive hematopoietic stem cells. *Leukemia* 2007; **21**: 1267–75.
25 Polli JW, Humphreys JE, Harmon KA *et al.* The role of efflux and uptake transporters in N-{3-chloro-4-[(3-fluorobenzyl)oxy]phenyl}-6-[5-({[2-(methylsulfonyl)ethyl]amino} methyl)-2-furyl]-4-quinazolinamine (GW572016, lapatinib) disposition and drug interactions. *Drug Metab Dispos* 2008; **36**: 695–701.
26 Shukla S, Robey RW, Bates SE, Ambudkar SV. Sunitinib (Sutent, SU11248), a small-molecule receptor tyrosine kinase inhibitor, blocks function of the ABC transporters, P-glycoprotein (ABCB1) and ABCG2. *Drug Metab Dispos* 2009; **37**: 359–65.
27 Dai CL, Liang YJ, Wang YS *et al.* Sensitization of ABCG2-overexpressing cells to conventional chemotherapeutic agent by sunitinib was associated with inhibiting the function of ABCG2. *Cancer Lett* 2009; **279**: 74–83.
28 Cusatis G, Gregorc V, Li J *et al.* Pharmacogenetics of ABCG2 and adverse reactions to gefitinib. *J Natl Cancer Inst* 2006; **98**: 1739–42.
29 McDowell HP, Meco D, Riccardi A *et al.* Imatinib mesylate potentiates topotecan antitumor activity in rhabdomyosarcoma preclinical models. *Int J Cancer* 2007; **120**: 1141–9.
30 Rudin CM, Liu W, Desai A *et al.* Pharmacogenomic and pharmacokinetic determinants of erlotinib toxicity. *J Clin Oncol* 2008; **26**: 1119–27.
31 van Erp NP, Eechoute K, van der Veldt AA *et al.* Pharmacogenetic pathway analysis for determination of sunitinib-induced toxicity. *J Clin Oncol* 2009; **27**: 4406–12.
32 Noguchi K, Kawahara H, Kaji A, Katayama K, Mitsuhashi J, Sugimoto Y. Substrate-dependent bidirectional modulation of P-glycoprotein-mediated drug resistance by erlotinib. *Cancer Sci* 2009; **100**: 1701–7.
33 Tamura A, Watanabe M, Saito H *et al.* Functional validation of the genetic polymorphisms of human ATP-binding cassette (ABC) transporter ABCG2: identification of alleles that are defective in porphyrin transport. *Mol Pharmacol* 2006; **70**: 287–96.
34 Miwa M, Tsukahara S, Ishikawa E, Asada S, Imai Y, Sugimoto Y. Single amino acid substitutions in the transmembrane domains of breast cancer resistance protein (BCRP) alter cross resistance patterns in transfectants. *Int J Cancer* 2003; **107**: 757–63.
35 Honjo Y, Hrycyna CA, Yan QW *et al.* Acquired mutations in the MXR/BCRP/ABCP gene alter substrate specificity in MXR/BCRP/ABCP-overexpressing cells. *Cancer Res* 2001; **61**: 6635–9.
36 Ozvegy-Laczka C, Koblos G, Sarkadi B, Varadi A. Single amino acid (482) variants of the ABCG2 multidrug transporter: major differences in transport capacity and substrate recognition. *Biochim Biophys Acta* 2005; **1668**: 53–63.
37 Morisaki K, Robey RW, Ozvegy-Laczka C *et al.* Single nucleotide polymorphisms modify the transporter activity of ABCG2. *Cancer Chemother Pharmacol* 2005; **56**: 161–72.
38 Hegedus T, Orfi L, Seprodi A, Varadi A, Sarkadi B, Keri G. Interaction of tyrosine kinase inhibitors with the human multidrug transporter proteins, MDR1 and MRP1. *Biochim Biophys Acta* 2002; **1587**: 318–25.
39 Ozvegy-Laczka C, Cserepes J, Elkind NB, Sarkadi B. Tyrosine kinase inhibitor resistance in cancer: role of ABC multidrug transporters. *Drug Resist Updat* 2005; **8**: 15–26.
40 Noguchi K, Katayama K, Mitsuhashi J, Sugimoto Y. Functions of the breast cancer resistance protein (BCRP/ABCG2) in chemotherapy. *Adv Drug Deliv Rev* 2009; **61**: 26–33.
41 Katayama K, Shibata K, Mitsuhashi J, Noguchi K, Sugimoto Y. Pharmacological interplay between breast cancer resistance protein and gefitinib in epidermal growth factor receptor signaling. *Anticancer Res* 2009; **29**: 1059–65.
42 Loo TW, Clarke DM. Mutational analysis of ABC proteins. *Arch Biochem Biophys* 2008; **476**: 51–64.
43 Saito H, Hirano H, Nakagawa H *et al.* A new strategy of high-speed screening and quantitative structure-activity relationship analysis to evaluate human ATP-binding cassette transporter ABCG2-drug interactions. *J Pharmacol Exp Ther* 2006; **317**: 1114–24.
44 Li YF, Polgar O, Okada M, Esser L, Bates SE, Xia D. Towards understanding the mechanism of action of the multidrug resistance-linked half-ABC transporter ABCG2: a molecular modeling study. *J Mol Graph Model* 2007; **25**: 837–51.
45 Hazai E, Bikadi Z. Homology modeling of breast cancer resistance protein (ABCG2). *J Struct Biol* 2008; **162**: 63–74.
46 Ozvegy-Laczka C, Varady G, Koblos G *et al.* Function-dependent conformational changes of the ABCG2 multidrug transporter modify its interaction with a monoclonal antibody on the cell surface. *J Biol Chem* 2005; **280**: 4219–27.

Supporting Information

Additional Supporting Information may be found in the online version of this article:

Fig. S1. Reversal of drug resistance by sunitinib. (a) Breast cancer resistance protein (BCRP)-mediated resistance to SN-38 (open circles) or mitoxantrone (MXR) (filled circles) in the presence of sunitinib was determined as IC_{50} values, and the relative resistance was calculated as the ratio of the IC_{50} value in the presence of sunitinib divided by the IC_{50} value in the absence of sunitinib. Similar analyses were performed for P-gp-mediated resistance to MXR (filled circles), doxorubicin (DOX) (filled triangles), vincristine (VCR) (open circles), and paclitaxel (PTX) (open diamonds) to investigate the effects of sunitinib (b) and cyclosporine A (CsA) (c).

Fig. S2. Positions of the substituted amino acids in the breast cancer resistance protein (BCRP) protein (a). Variant BCRP protein expression levels were analyzed by western blotting (b) and flow cytometry (c) in selected *BCRP*-transduced PA317 cells. For western blotting, cell lysates (10 μg/lane) were resolved by SDS-PAGE and the expression of BCRP and GAPDH was detected using anti-BCRP (3488) or anti-GAPDH antibodies, respectively. For FACS analysis, cells were incubated with or without a biotinylated anti-BCRP 5D3 antibody, and labeled with R-phycoerythrin-conjugated streptavidin.

Fig. S3. Binding of the 5D3 antibody to F431L-breast cancer resistance protein (BCRP). Interactions between sunitinib and BCRP were monitored with the 5D3 reactivity change, as described in the Materials and Methods. The cells were incubated in the presence or absence of 1, 3, and 10 μmol/L FTC for 5 min at 37°C followed by incubation with the 5D3 antibody (2 μg/mL) for 1 h at 37°C. After incubation with the secondary antibody, the cells were washed and fluorescence intensity was measured using a BDTM LSR II system.

Please note: Wiley-Blackwell are not responsible for the content or functionality of any supporting materials supplied by the authors. Any queries (other than missing material) should be directed to the corresponding author for the article.

doi: 10.1111/j.1349-7006.2010.01539.x

Biochemical and Biophysical Research Communications 394 (2010) 569–573

Contents lists available at ScienceDirect

Biochemical and Biophysical Research Communications

journal homepage: www.elsevier.com/locate/ybbrc

A novel yeast cell-based screen identifies flavone as a tankyrase inhibitor

Yoko Yashiroda [a,*], Reika Okamoto [a,b], Kaori Hatsugai [c,d], Yasushi Takemoto [a], Naoki Goshima [e], Tamio Saito [f], Makiko Hamamoto [g], Yoshikazu Sugimoto [d], Hiroyuki Osada [f], Hiroyuki Seimiya [c], Minoru Yoshida [a,h]

[a] Chemical Genomics Research Group/Chemical Genetics Laboratory, RIKEN Advanced Science Institute, Wako, Saitama 351-0198, Japan
[b] Japan Biological Informatics Consortium (JBIC), Koto-ku, Tokyo 135-8073, Japan
[c] Division of Molecular Biotherapy, Cancer Chemotherapy Center, Japanese Foundation for Cancer Research, Koto-ku, Tokyo 135-8550, Japan
[d] Division of Chemotherapy, Graduate School of Pharmaceutical Sciences, Keio University, Minato-ku, Tokyo 105-8512, Japan
[e] National Institute of Advanced Industrial Science and Technology, Koto-ku, Tokyo 135-0064, Japan
[f] Chemical Biology Core Facility/Antibiotics Laboratory, RIKEN Advanced Science Institute, Wako, Saitama 351-0198, Japan
[g] Department of Life Sciences, School of Agriculture, Meiji University, Kawasaki, Kanagawa 214-8571, Japan
[h] CREST Research Project, Japan Science and Technology Corporation, Saitama 332-0012, Japan

ARTICLE INFO

Article history:
Received 23 February 2010
Available online 7 March 2010

Keywords:
Tankyrase 1
Inhibitor
High-throughput screening
Schizosaccharomyces pombe

ABSTRACT

The telomere-associated protein tankyrase 1 is a poly(ADP-ribose) polymerase and is considered to be a promising target for cancer therapy, especially for BRCA-associated cancers. However, an efficient assay system for inhibitor screening has not been established, mainly due to the difficulty of efficient preparation of the enzyme and its substrate. Here, we report a cell-based assay system for detecting inhibitory activity against tankyrase 1. We found that overexpression of the human tankyrase 1 gene causes a growth defect in the fission yeast *Schizosaccharomyces pombe*. Chemicals that restore the growth defect phenotype can be identified as potential tankyrase 1 inhibitors. We performed a high-throughput screen using this system, and identified flavone as a compound that restores the growth of yeast cells overexpressing tankyrase 1. Indeed, flavone inhibited poly(ADP-ribosyl)ation of proteins caused by overexpression of tankyrase 1 in yeast cells. This system allows rapid identification of inhibitory activity against tankyrase 1 and is amenable to high-throughput screening using robotics.

1. Introduction

Poly(ADP-ribose) polymerases (PARPs) catalyze the covalent attachment of poly(ADP-ribose) (PAR) polymers to a protein substrate. PAR polymers are assembled from monomers of the enzyme's substrate, nicotinamide adenine dinucleotide (NAD^+). The PARP family includes at least 17 family members, which are involved in a wide range of cellular processes [1]. One family member, tankyrase 1 (TRF1-interacting ankyrin-related ADP-ribose polymerase 1) was originally identified in a yeast two-hybrid screen as a protein binding to telomeric repeat binding factor, TRF1 [2,3]. Telomeres are the unique DNA–protein complexes at the eukaryotic chromosome ends. TRF1 binds to the telomeric DNA and negatively regulates telomere length [4]. Tankyrase 1 poly(ADP-ribosyl)ates TRF1, releasing TRF1 from telomere DNA and stimulating ubiquitin-mediated proteolysis of TRF1 [5]. Thus, tankyrase 1 is a positive regulator of telomere length. In human, germ cells and most cancer cells exhibit a high level of telomerase activity that maintains telomere length, allowing these cells to divide indefinitely [6,7]. Therefore, telomerase is one of the attractive targets for cancer therapy. To date, several telomerase inhibitors have been developed and reported (e.g., GRN163L and MST-312) [8,9]. In this context, tankyrase 1, another positive regulator of telomeres, is also a potential target for telomere-directed anticancer therapeutics. A recent report showed that inhibition of tankyrase 1 was lethal only when combined with BRCA (breast cancer associated) deficiency. Loss of BRCA function is associated with breast cancer as well as malignancies of the ovaries, pancreas, and prostate gland [10]. This synthetic lethal interaction is an attractive therapeutic approach because treatment with a single agent that targeted tankyrase 1 would be expected to specifically kill cancer cells, but not most normal cells. Prior to the proposal of targeting tankyrase 1 as a therapeutic strategy for BRCA-associated cancer, inhibition of the DNA repair enzyme PARP1 was known to show selective toxicity against BRCA-deficient cells [11,12]. However, due to patients' refractoriness to PARP1 inhibitors or acquisition of drug resistance, it became important to identify alternative therapeutic targets for BRCA-associated cancers. Therefore, the development of tankyrase 1 inhibitors is a promising approach to anticancer therapeutics. Recently, XAV939 was identified as a tankyrase inhibitor during screening for a small-molecule

* Corresponding author. Address: Chemical Genetics Laboratory, RIKEN Advanced Science Institute, 2-1 Hirosawa, Wako, Saitama 351-0198, Japan. Fax: +81 48 462 1749.
E-mail address: ytyy@riken.jp (Y. Yashiroda).

0006-291X/$ - see front matter © 2010 Elsevier Inc. All rights reserved.
doi:10.1016/j.bbrc.2010.03.021